

MODELING ADAGRAD, RMSPROP, AND ADAM WITH INTEGRO-DIFFERENTIAL EQUATIONS

Carlos Heredia*

*IAMM Research, Department of Applied Artificial Intelligence
DAMM, Carrer del Rosselló 515, 08025 Barcelona, Catalonia, Spain*

ABSTRACT

In this paper, we propose a continuous-time formulation for the AdaGrad, RMSProp, and Adam optimization algorithms by modeling them as first-order integro-differential equations. We perform numerical simulations of these equations, along with stability and convergence analyses, to demonstrate their validity as accurate approximations of the original algorithms. Our results indicate a strong agreement between the behavior of the continuous-time models and the discrete implementations, thus providing a new perspective on the theoretical understanding of adaptive optimization methods.

Keywords: Adaptive Optimization Algorithms, Integro-differential Equations, Machine Learning.

1 INTRODUCTION

Central to numerous machine learning tasks is the challenge of solving the following optimization problem:

$$\arg \min_{\theta \in \mathbb{R}^n} f(\theta),$$

where $f : \mathbb{R}^n \rightarrow \mathbb{R}$ denotes a typically non-convex and differentiable objective (or loss) function. The pursuit of finding the global minima of such functions presents a significant challenge due to the inherent complexity and non-convexity of the landscape.

Gradient Descent (GD) remains one of the most prominent algorithms for minimizing the function f by iteratively finding the optimal parameters θ Boyd & Vandenberghe (2004). It operates by adjusting the parameters in the direction of the steepest descent of f with a fixed step size α (learning rate). At each iteration, the algorithm computes the gradient of f with respect to θ , guiding the parameter updates to minimize f progressively Rumelhart et al. (1986):

$$\theta_t \leftarrow \theta_{t-1} - \alpha \nabla_{\theta} f_t(\theta_{t-1}). \quad (1)$$

While Stochastic Gradient Descent (SGD) Bottou (2010) extends the Gradient Descent method by using mini-batches, or randomly selected subsets of data, to compute gradients, this article focuses on a non-stochastic perspective. The continuous nature of these methods permits a more direct application of differential equation techniques, as we demonstrate in Section 4. For readers interested in a continuous description of the stochastic method, we refer to Sirignano & Spiliopoulos (2017).

Adaptive optimization methods such as AdaGrad Duchi et al. (2011) and RMSProp Hinton (2012) have been pivotal in advancing gradient-based algorithms. AdaGrad adapts the learning rate for each parameter by accumulating the sum of past squared gradients, which can lead to a significant decrease in the learning rate over time. In contrast, RMSProp mitigates this issue by maintaining an exponentially weighted average of squared gradients, ensuring a more stable learning process. These innovations laid the groundwork for more sophisticated algorithms like Adam.

Adam (Adaptive Moment Estimation) Kingma & Ba (2014) refines gradient descent by computing adaptive learning rates for each parameter, leveraging both the first moment and the second moment of the gradients. Variants like AdamW Loshchilov & Hutter (2017) and AdamL2 have been proposed to address specific issues such as weight decay and improved regularization.

*e-mail address: carlosherediapimienta@gmail.com

To analyze these optimization algorithms through a continuous framework, we employ well-established tools from differential equations to examine the convergence and stability of these methods. For example, as the learning rate tends to zero ($\alpha \rightarrow 0$), the gradient descent algorithm, interpreted via the Euler method, can be approximated by the following first-order differential equation:

$$\dot{\theta} = -\nabla_{\theta} f(\theta).$$

Given that the AdaGrad, RMSProp, and Adam algorithms incorporate memory effects through the accumulation of past gradients, they are naturally expected to be represented by integro-differential operators. The primary contributions of this work are summarized as follows:

- We propose continuous formulations for the AdaGrad, RMSProp, and Adam algorithms using integro-differential equations, as described in Propositions 1 to 3. We emphasize that the memory effects are encapsulated within the nonlocal terms of these equations.
- We prove the stability of these integro-differential equations, as well as their convergence rates. Theorems 1 to 6.
- We provide a numerical comparison between the results obtained from these continuous models and the original discrete algorithms, focusing on the accuracy and dynamics of the continuous approximations: Figures 1 to 15. Additionally, we detail the numerical methods employed to solve the integro-differential equations.

This article is organized as follows:

- Sec. 2. Optimization Algorithms.** We review the AdaGrad, RMSProp, and Adam algorithms.
- Sec. 3. Continuous Representations.** We introduce the continuous versions of these algorithms as first-order integro-differential equations.
- Sec. 4. Convergence and Stability Analysis.** We establish stability and convergence theorems for these continuous nonlocal models
- Sec. 5. Numerical Simulations.** We compare the numerical results obtained from these continuous models with those from the discrete algorithms, and we provide a detailed explanation of the numerical method used to solve the integro-differential equations.

1.1 NOTATION

In this subsection, we introduce and define the notation used throughout Section 2 and 3. Although the notation may appear “highly” physical, it is adopted here for its simplicity and ease when presenting the results.

Our discussion is set within an n -dimensional Euclidean space, and the key elements of the notation are as follows:

- **Parameter Space:** The parameters θ are represented as vectors in \mathbb{R}^n , where \mathbb{R} denotes the set of real numbers. These parameters are assumed to be differentiable functions.
- **Euclidean Metric:** The Euclidean metric δ_{ij} is employed to raise and lower indices, where δ_{ij} is the Kronecker delta.
- **Einstein Summation Convention:** We adopt the Einstein summation convention, wherein repeated indices imply summation over the corresponding index range. For example:

$$\theta^2 := \|\theta\|^2 := \theta_i \theta^i = \delta_{ij} \theta^i \theta^j = \sum_{i=1}^n \theta^i \theta^i,$$

which represents the squared Euclidean norm of the vector θ .

- **Derivative Notation:** The partial derivative with respect to the i -th component of θ is denoted by ∂_i . Specifically, the gradient operator is expressed as:

$$\nabla_{\theta} = (\nabla_1, \dots, \nabla_i, \dots, \nabla_n) = \left(\frac{\partial}{\partial \theta^1}, \dots, \frac{\partial}{\partial \theta^i}, \dots, \frac{\partial}{\partial \theta^n} \right) := (\partial_1, \dots, \partial_i, \dots, \partial_n).$$

In Section 4, we use the traditional notation used in optimization textbooks, where $\langle \cdot, \cdot \rangle$ denotes the scalar product in the n -dimensional Euclidean space, as we wish to adhere as closely as possible to standard mathematical notation.

1.2 RELATED WORK

Adaptive optimization algorithms like AdaGrad, RMSProp, and Adam are widely adopted in deep learning due to their robustness and efficiency. However, the inherently discrete nature of deep learning algorithms has led researchers to explore continuous representations to gain deeper theoretical insights and leverage mathematical tools from continuous dynamical systems.

Continuous Representations: Researchers have extended discrete optimization algorithms to continuous settings using differential equations. For instance, Su et al. (2016) provide a theoretical framework that connects Nesterov’s accelerated gradient method with a second-order ordinary differential equation (ODE), offering insights into the convergence properties and dynamics of optimization algorithms. Similarly, Wibisono et al. (2016) present a variational perspective on accelerated methods by deriving ODEs using a Lagrangian framework, capturing the essence of momentum in optimization.

These continuous formulations allow for the analysis of optimization dynamics and convergence properties, such as asymptotic Lyapunov stability Gantmakher (1970). Stability analysis helps determine whether the solutions of optimization algorithms remain near an equilibrium point or diverge over time, providing deeper insights into their robustness Khalil (2002). Additionally, Romero et al. (2022) focus on the challenge of discretizing continuous-time analogues of optimization algorithms, particularly gradient-based methods, while retaining the optimality properties inherent in the continuous formulation.

Extending this continuous perspective to neural networks, Chen et al. (2018) introduce Neural Ordinary Differential Equations (Neural ODEs), which model the evolution of hidden states in continuous time, bridging the gap between discrete neural networks and continuous dynamical systems. Similarly, Ruthotto & Haber (2020) explore how partial differential equations (PDEs) can be used to model and design deep neural networks. By interpreting layers in a neural network as time steps in a PDE solver, they provide a continuous-time perspective that can lead to new architectures and training algorithms, such as parabolic, elliptic, and hyperbolic CNNs.

On another front, Li et al. (2017) explore stochastic gradient algorithms through stochastic differential equations (SDEs), providing a deeper understanding of their behavior in the continuous limit. This perspective is valuable for analyzing the convergence and stability properties of stochastic optimization methods.

Integro-Differential Equations and Memory Effects: Recent research has examined the use of integro-differential equations (IDEs) to model biological and physical processes, as they can more accurately capture memory and cumulative effects than ODEs. For instance, Zappala et al. (2022) introduce Neural Integro-Differential Equations, combining neural networks with IDEs to model systems where both past and future states influence the current state. This approach is particularly effective in extrapolating temporal data and generalizing to unseen initial conditions, providing a framework for modeling complex dynamics with nonlocal interactions.

Physical Perspectives on Optimization: Weinan E (2017) suggests rethinking machine learning algorithms through the lens of dynamical systems and control theory. In this view, optimization algorithms are modeled as continuous-time dynamical systems, treating learning as a control problem where parameters are adjusted for optimal outcomes. He also proposes that this continuous framework makes it possible to apply advanced control techniques, such as adaptive time-stepping, Hamiltonian structures, and constraints, to improve the efficiency and stability of machine learning models.

In this context, departing from traditional neural networks that focus on learning mappings between inputs and outputs, Hamiltonian Neural Networks (HNNs) Greydanus et al. (2019) and Lagrangian Neural Networks (LNNs) Cranmer et al. (2020) incorporate fundamental physical principles directly into their architectures. HNNs are rooted in Hamiltonian mechanics and are trained to learn a Hamiltonian function that inherently respects exact conservation laws in an unsupervised manner. This approach makes them particularly effective for modeling systems where energy conservation is critical, such as the two-body problem. Conversely, LNNs employ the Euler-Lagrange equations by parameterizing arbitrary Lagrangian functions using neural networks without requiring canonical

coordinates. This capability enables LNNs to perform well in situations where canonical momenta are unknown or difficult to compute.

Noether’s theorem, which establishes a fundamental connection between symmetries and conserved quantities in physical systems, has also inspired advancements in machine learning. For example, Noether Networks Alet et al. (2021) leverage this theorem to meta-learn conserved quantities, improving prediction quality in sequential problems. Furthermore, Tanaka & Kunin (2021) develop a theoretical framework to study the geometry of learning dynamics in neural networks, revealing a key mechanism of explicit symmetry breaking behind the efficiency and stability of modern neural networks.

While previous works have successfully employed ordinary differential equations (ODEs) and partial differential equations (PDEs) to model optimization algorithms and neural networks, they often focus on methods without explicit memory terms or cumulative effects. Our work distinguishes itself by proposing continuous formulations of AdaGrad, RMSProp, and Adam using integro-differential equations. By explicitly modeling the memory effects inherent in these adaptive algorithms through integral operators, we provide a novel perspective that captures their nonlocal dynamics. This distinction is crucial for achieving a deeper theoretical understanding and for developing new optimization strategies inspired by nonlocal behaviors, setting our work apart from prior studies that model optimization algorithms solely as ODEs.

Therefore, our approach allows us to: (a) accurately represent cumulative effects by directly modeling how past gradients influence current updates—a defining characteristic of adaptive optimization algorithms; (b) facilitate theoretical analysis, as the continuous framework enables the application of advanced mathematical tools from the theory of integro-differential equations, such as stability analysis and convergence proofs; and (c) bridge discrete and continuous dynamics, offering insights into the behavior of these algorithms and potential improvements.

2 OPTIMIZATION ALGORITHMS

In this section, we present the optimization algorithms¹: AdaGrad, RMSProp, and Adam, with the aim of illustrating the evolution of the parameters as they converge towards the minimum of two representative toy models. The first model is a convex and differentiable function,

$$f(\theta) = (\theta - 4)^2,$$

chosen for its simplicity and for having a known minimum at $\theta = 4$, which allows for straightforward analytical determination and facilitates direct comparisons with numerical simulations.

To complement this, we also consider a non-convex toy model,

$$f(\theta) = \frac{1}{4}(\theta^2 - 1)^2,$$

which exhibits multiple local minima, $\theta = \pm 1$, and an unstable critical point (a local maxima) at $\theta = 0$. With these two toy models, we can analyze the dynamics of the continuous-time formulations in both convex and non-convex regimes.

2.1 FUNDAMENTALS OF ADAGRAD

The Adaptive Gradient Algorithm (AdaGrad), introduced by Duchi et al. (2011), marks a significant advancement in the development of optimization techniques. The primary innovation of AdaGrad is its ability to adapt the learning rate for each parameter individually, based on the historical gradients observed during training.

AdaGrad is distinguished by maintaining a cumulative sum of the squares of past gradients for each parameter, denoted as $G_{k,i}$. This accumulation effectively scales the learning rate inversely proportional to the square root of $\text{diag}(G_{k,i})$, ensuring that parameters frequently updated receive smaller updates, while parameters updated less frequently receive larger updates. This particular

¹For a comprehensive overview of Gradient Descent optimization algorithms, see Ruder (2016).

variant of AdaGrad is known as AdaGrad-Diagonal. However, for simplicity of analysis, in this work we focus on the AdaGrad-Norm variant, in which all parameters are scaled uniformly, namely, G_k .

A notable strength of AdaGrad is its capability to handle scenarios involving sparse features, as it allows for larger updates for parameters associated with infrequent features. However, a limitation arises when the accumulated gradient sum G_k increases excessively over time, causing the effective learning rate to diminish and potentially leading to premature convergence or slower learning. As will be discussed, this issue is mitigated by the RMSProp algorithm.

Mathematical Formulation of AdaGrad: Consider an objective function $f : \mathbb{R}^n \rightarrow \mathbb{R}$, parameterized by $\theta \in \mathbb{R}^n$, with a learning rate $\alpha \in (0, 1]$. AdaGrad iteratively updates the parameters as described in Algorithm 1, where ϵ is a small constant added to prevent division by zero (typically $\sim 10^{-8}$), and k denotes the current timestep.

Algorithm 1 AdaGrad Optimization Algorithm

- 1: Initialize parameters $\theta_{k=0}^i$ and the accumulated squared gradient sum $G_{k=0} = 0$.
 - 2: **while** the parameters θ_k^i have not converged **do**
 - 3: $k \leftarrow k + 1$
 - 4: Compute the gradient: $g_k^i \leftarrow \delta^{ij} \partial_j f(\theta_{k-1})$.
 - 5: Accumulate gradients: $G_k \leftarrow G_{k-1} + g_k^2$
 - 6: Update parameters: $\theta_k^i \leftarrow \theta_{k-1}^i - \alpha g_k^i / (\sqrt{G_k} + \epsilon)$
 - 7: **end while**
-

2.2 FUNDAMENTALS OF RMSPROP

The Root Mean Square Propagation (RMSProp) optimizer, introduced by Hinton in his lecture series Hinton (2012), was developed primarily to address the issue of diminishing learning rates encountered in AdaGrad, which can slow down convergence over time.

RMSProp distinguishes itself by maintaining a moving average of the squared gradients for each parameter, denoted as v . This method allows the algorithm to adaptively adjust the learning rate based on the recent magnitude of the gradients, effectively preventing the learning rate from becoming excessively small. The moving average is computed using an exponential decay rate β , which determines the influence of recent gradients on the current value of v . A β value close to 1 reduces the impact of recent gradients, resulting in a smoother and more stable average.

A key advantage of RMSProp is its ability to maintain a more consistent learning rate throughout the optimization process. By avoiding the drastic reduction in learning rates seen in AdaGrad, RMSProp allows for more sustained and effective learning over time.

Mathematical Formulation of RMSProp: Consider an objective function $f : \mathbb{R}^n \rightarrow \mathbb{R}$, parameterized by $\theta \in \mathbb{R}^n$, and an exponential decay rate $\beta \in [0, 1)$. RMSProp iteratively updates the parameters as described in Algorithm 2, where $\alpha \in (0, 1]$ denotes the learning rate, ϵ is a small constant to prevent division by zero (typically $\sim 10^{-8}$), and k is the current timestep.

Algorithm 2 RMSProp Optimization Algorithm

- 1: Initialize parameters $\theta_{k=0}^i$ and the squared gradient moving average $v_{k=0} = 0$.
 - 2: **while** the parameters θ_k^i have not converged **do**
 - 3: $k \leftarrow k + 1$
 - 4: Compute the gradient: $g_k^i \leftarrow \delta^{ij} \partial_j f(\theta_{k-1})$.
 - 5: Update the squared gradient moving average: $v_k \leftarrow \beta v_{k-1} + (1 - \beta) g_k^2$
 - 6: Update parameters: $\theta_k^i \leftarrow \theta_{k-1}^i - \alpha g_k^i / (\sqrt{v_k} + \epsilon)$
 - 7: **end while**
-

2.3 FUNDAMENTALS OF ADAM

The Adaptive Moment Estimation (Adam) optimizer, introduced by Kingma and Ba (2014) Kingma & Ba (2014), represents also a significant advancement in optimization techniques, particularly in the fields of deep learning. It combines the strengths of two other gradient-based optimization methods: the Adaptive Gradient Algorithm and Root Mean Square Propagation.

Adam distinguishes itself by maintaining two separate moving averages for each parameter: the first moment, m^i , and the second moment, v . The first moment estimates the gradients, while the second moment estimates the squared gradients, similar to RMSProp's adaptive learning rates. These moving averages are computed using exponential decay rates, β_1 and β_2 , respectively.

Values of β_1 and β_2 close to 1 imply a longer memory of past gradients, effectively smoothing the averages over a larger number of iterations. This smoothing helps stabilize the optimization process by reducing the impact of sudden changes in gradient values.

Mathematical Formulation of Adam: Consider an objective function $f : \mathbb{R}^n \rightarrow \mathbb{R}$, parameterized by $\theta \in \mathbb{R}^n$, with exponential decay rates $\beta_1, \beta_2 \in [0, 1]$. Adam iteratively updates the parameters as described in Algorithm 3, where $\alpha \in (0, 1]$ denotes the learning rate, ϵ is a small constant to prevent division by zero (typically $\sim 10^{-8}$), and k is the current timestep.

Algorithm 3 Adam Optimization Algorithm

- 1: Initialize the parameters $\theta_{k=0}^i$, the first moment $m_{k=0}^i = 0$, and the second moment $v_{k=0} = 0$.
 - 2: **while** the parameters θ_k^i have not converged **do**
 - 3: $k \leftarrow k + 1$
 - 4: Compute the gradient: $g_k^i \leftarrow \delta^{ij} \partial_j f(\theta_{k-1})$.
 - 5: Update first moment: $m_k^i \leftarrow \beta_1 m_{k-1}^i + (1 - \beta_1) g_k^i$
 - 6: Update second moment: $v_k \leftarrow \beta_2 v_{k-1} + (1 - \beta_2) g_k^2$
 - 7: Correct first moment: $\hat{m}_k^i \leftarrow m_k^i / (1 - \beta_1^k)$
 - 8: Correct second moment: $\hat{v}_k \leftarrow v_k / (1 - \beta_2^k)$
 - 9: Update parameters: $\theta_k^i \leftarrow \theta_{k-1}^i - \alpha \hat{m}_k^i / (\sqrt{\hat{v}_k} + \epsilon)$
 - 10: **end while**
-

3 CONTINUOUS-TIME MODELS FOR ADAGRAD, RMSPROP AND ADAM

Expressing the optimizers discussed in the previous section within a continuous framework offers several advantages, particularly by enhancing the understanding and analysis of their temporal behavior. Continuous formulations allow the application of advanced mathematical tools, such as Lyapunov stability analysis, to investigate the dynamics of parameter updates and the convergence properties of the algorithm Kovachki & Stuart (2021).

Next, we present three propositions (three continuous-time models) for the optimization algorithms AdaGrad, RMSProp, and Adam. In all cases, we assume the following conditions:

Assumption 1. *The relationship between the temporal variable t and the iteration k is governed by the learning rate α such that*

$$t = \alpha k. \quad (2)$$

Building on this assumption,

Assumption 2. *Given a small learning rate α , the timescale relationship is expressed as:*

$$z_{\frac{t+\alpha}{\alpha}}^i := z^i(t + \alpha) \sim z^i(t) + \alpha \dot{z}^i(t) + \mathcal{O}(\alpha^2) \quad \text{and} \quad z_{\frac{t}{\alpha}}^i := z^i(t) \quad \text{for} \quad t > 0.$$

Therefore,

Proposition 1 (Nonlocal Continuous Dynamics of AdaGrad). *Under Assumptions 1 and 2, and with an initial value for the accumulated gradients $G_0 = 0$, the continuous nonlocal dynamics of AdaGrad can be characterized by the following equation:*

$$\dot{\theta}^i(t) = - \frac{\partial^i f(\theta)}{\sqrt{G(t + \alpha, \theta)} + \epsilon}, \quad (3)$$

where ϵ is a small real value (typically $\sim 10^{-8}$), and the nonlocal term $G(t, \theta)$ is defined as:

$$G(t, \theta) = \frac{1}{\alpha} \int_0^t d\tau \partial^i f(\theta(\tau)) \partial_i f(\theta(\tau)).$$

Proof. To facilitate the proof, we begin by shifting the temporal indexing from $k \leftarrow k + 1$ to $k + 1 \leftarrow k$. Consequently, the parameter update rule becomes:

$$\theta_{k+1}^i = \theta_k^i - \alpha \frac{\partial^i f(\theta_k)}{\sqrt{G_{k+1}} + \epsilon}.$$

By applying Assumption 2, the evolution of the accumulated gradients can be described by the differential equation:

$$\dot{G}(t, \theta) = \frac{1}{\alpha} \partial^i f(\theta) \partial_i f(\theta),$$

whose solution (for $t > 0$) is:

$$G(t, \theta) = \frac{1}{\alpha} \int_0^t d\tau \partial^i f(\theta(\tau)) \partial_i f(\theta(\tau)).$$

Using Assumption 2 again, we derive the integro-differential equation that governs the updated parameters:

$$\dot{\theta}^i(t) = -\frac{\partial^i f(\theta)}{\sqrt{G(t + \alpha, \theta)} + \epsilon}.$$

□

This proposition highlights that the continuous-time model for AdaGrad is described by a first-order integro-differential equation. Notice that the nonlocality is embedded in the accumulated gradient term, where the entire trajectory of θ up to time t must be known, along with a small differential time step (future) described by α .

Now, we introduce the continuous model for RMSProp. Hence,

Proposition 2 (Nonlocal Continuous Dynamics of RMSProp). *Under Assumptions 1 and 2, and given an initial value for the squared gradient moving average $v_0 = 0$, the continuous nonlocal dynamics of RMSProp can be characterized by the following equation:*

$$\dot{\theta}^i(t) = -\frac{\partial^i f(\theta)}{\sqrt{v(t + \alpha, \theta)} + \epsilon}, \quad (4)$$

where ϵ is a small real value (typically $\sim 10^{-8}$), and the nonlocal term $v(t, \theta)$ is defined as:

$$v(t, \theta) = \frac{1 - \beta}{\alpha} \int_0^t d\tau e^{-\frac{1-\beta}{\alpha}(t-\tau)} \partial^i f(\theta(\tau)) \partial_i f(\theta(\tau)).$$

Proof. To simplify the proof, as in Proposition 1, we shift the indexing such that $k + 1 \leftarrow k$. The parameter update then becomes:

$$\theta_{k+1}^i = \theta_k^i - \alpha \frac{\partial^i f(\theta_k)}{\sqrt{v_{k+1}} + \epsilon}.$$

By applying Assumption 2, the evolution of the squared gradient moving average is governed by the differential equation:

$$\dot{v} + \frac{1 - \beta}{\alpha} v = \frac{1 - \beta}{\alpha} \partial^i f(\theta) \partial_i f(\theta). \quad (5)$$

Rewriting this equation yields:

$$\frac{d}{dt} \left[e^{\frac{1-\beta}{\alpha} t} v \right] = \frac{1 - \beta}{\alpha} e^{\frac{1-\beta}{\alpha} t} \partial^i f(\theta) \partial_i f(\theta), \quad (6)$$

which leads to the solution (for $t > 0$):

$$v(t, \theta) = \frac{1 - \beta_2}{\alpha} \int_0^t d\tau e^{-\frac{1-\beta_2}{\alpha}(t-\tau)} \partial^i f(\theta(\tau)) \partial_i f(\theta(\tau)). \quad (7)$$

Finally, by applying Assumption 2, the parameter updates follow the integro-differential equation:

$$\dot{\theta}^i(t) = -\frac{\partial^i f(\theta)}{\sqrt{v(t + \alpha, \theta) + \epsilon}}. \quad (8)$$

□

As discussed earlier, a similar situation arises with RMSProp: the dynamics are governed by the integro-differential equation (4). The nonlocal behavior is encapsulated within the squared gradient moving average. It is necessary to know the value of θ up to time t and a small time increment determined by α .

The key difference between RMSProp and AdaGrad lies in the kernel of the integral operator. For AdaGrad, the kernel is

$$K_{AG}(t) = \frac{1}{\alpha}.$$

However, for RMSProp, the kernel is modified to:

$$K_{RP}(t) = \frac{1 - \beta}{\alpha} e^{-\frac{1-\beta}{\alpha}t}.$$

Finally, we introduce the continuous model for Adam:

Proposition 3 (Nonlocal Continuous Dynamics of Adam). *Under Assumption 2 and 1, and with initial values for the moments $m_0^i = 0$ and $v_0 = 0$, the Adam optimizer can be characterized by the following continuous nonlocal dynamics:*

$$\dot{\theta}^i(t) = -\alpha(t) \frac{m^i(t, \theta)}{\sqrt{v(t, \theta) + \epsilon(t)}}, \quad (9)$$

where

$$\alpha(t) = \frac{\sqrt{1 - \beta_2^{\frac{t}{\alpha}}}}{1 - \beta_1^{\frac{t}{\alpha}}}, \quad \text{and} \quad \epsilon(t) = \epsilon \sqrt{1 - \beta_2^{\frac{t}{\alpha}}}, \quad (10)$$

and the moments are given by:

$$m^i(t, \theta) = \int_0^t d\tau K_1(t-\tau) \partial^i f(\theta(\tau)), \quad \text{and} \quad v(t, \theta) = \int_0^t d\tau K_2(t-\tau) \partial^i f(\theta(\tau)) \partial_i f(\theta(\tau)),$$

with the kernel function $K_a(t)$ defined as:

$$K_a(t) = \frac{1 - \beta_a}{\alpha} e^{-\frac{1-\beta_a}{\alpha}t}, \quad a = 1, 2.$$

Proof. To prove this proposition, we start from step 5-6 of Algorithm 3: $m_k^i = \beta_1 m_{k-1}^i + (1 - \beta_1) g_k^i$ and $v_k = \beta_2 v_{k-1} + (1 - \beta_2) g_k^2$. Since the structure is identical for both moments, we demonstrate the process for one, knowing the other will follow similarly, except for differences in the exponential decay or gradient. We redefine the indices as $k + 1 \leftarrow k$ to avoid involving θ_{t-1} in the gradient.

Focusing on the second moment v , we use the same approach as in Proposition 2 to obtain:

$$v(t, \theta) = \frac{1 - \beta_2}{\alpha} \int_0^t d\tau e^{-\frac{1-\beta_2}{\alpha}(t-\tau)} \partial^i f(\theta(\tau)) \partial_i f(\theta(\tau)). \quad (11)$$

The first moment $m^i(t, \theta)$ follows a similar pattern, differing by the absence of the squared gradient and the exponential decay factor β_2 :

$$m^i(t, \theta) = \frac{1 - \beta_1}{\alpha} \int_0^t d\tau e^{-\frac{1-\beta_1}{\alpha}(t-\tau)} \partial^i f(\theta(\tau)). \quad (12)$$

Applying Assumptions 2 and 1 and performing some algebraic manipulations yields:

$$\dot{\theta}^i(t) = -\alpha(t) \frac{m^i(t, \theta)}{\sqrt{v(t, \theta) + \epsilon(t)}}, \quad (13)$$

where

$$\alpha(t) = \frac{\sqrt{1 - \beta_2^{\frac{t}{\alpha}}}}{1 - \beta_1^{\frac{t}{\alpha}}}, \quad \text{and} \quad \epsilon(t) = \epsilon \sqrt{1 - \beta_2^{\frac{t}{\alpha}}}. \quad (14)$$

□

In the case of Adam, the nonlocality is encapsulated within both moments, as expected. A key distinction between Adam and other optimizers such as AdaGrad or RMSProp (beyond the use of the exponential decay rates, β_1 and β_2 , and the specific kernel structure in AdaGrad) is that Adam does not require incorporating the future time differential α that was necessary in the other cases; namely, it is evaluated at the same instant t , so the nonlocality enters only through m and v , without any shift to $t + \alpha$.

These propositions confirm that the accumulative effects present in adaptive algorithms such as AdaGrad, RMSProp, and Adam are represented in continuous form as integro-differential equations (or nonlocal equations), where the presence of the kernel in the integral operator regulates the influence of the gradient on the dynamics.

4 THEORETICAL FRAMEWORK FOR CONTINUOUS-TIME DYNAMICS

Thanks to the continuous-time formulation of these algorithms, we can investigate their convergence and stability properties using mathematical tools such as Lyapunov or LaSalle stability analysis and convergence theory for both convex and non-convex objective functions. To enhance clarity, this section is divided into two parts: the first focuses on convex functions, while the second addresses non-convex functions.

4.1 GENERAL ASSUMPTIONS

To begin, we assume that $f : \mathbb{R}^n \rightarrow \mathbb{R}$ is of class \mathcal{C}^1 . We denote by $\theta(t) \in \mathbb{R}^n$ the continuous-time trajectory of the parameter, and by $g_i(t) := \nabla_i f(\theta(t))$ the gradient evaluated along this trajectory. Furthermore, in order to represent compactly the kernels of the integral operators appearing in the integro-differential equations, we introduce the following definition.

Definition 1. *Let ν be a finite Borel measure on $[0, \infty)$. We define the kernel function*

$$K_\nu(t) := \int_{[0, \infty)} e^{-\lambda t} d\nu(\lambda), \quad t \geq 0. \quad (15)$$

Given a function $g : [0, \infty) \rightarrow \mathbb{R}^n$ that is measurable and locally integrable, the associated memory operator is defined as

$$M_{\nu, i}[g](t) := \int_0^t K_\nu(t - \tau) g_i(\tau) d\tau. \quad (16)$$

Lemma 1. *Let $\alpha > 0$ and $\beta_a \in [0, 1)$. If*

$$\nu_{\text{AG}} = \frac{1}{\alpha} \delta_0, \quad \nu_{\text{RM/Adam}} = \frac{1 - \beta_a}{\alpha} \delta_{\frac{1 - \beta_a}{\alpha}}, \quad (17)$$

then the corresponding kernels defined in Definition 1 are

$$K_{\nu_{\text{AG}}}(t) = \frac{1}{\alpha}, \quad K_{\nu_{\text{RM/Adam}}}(t) = \frac{1 - \beta_a}{\alpha} e^{-\frac{1 - \beta_a}{\alpha} t}, \quad (18)$$

where δ_a denotes the Dirac measure, i.e.,

$$\delta_a(B) = \begin{cases} 1, & \text{if } a \in B, \\ 0, & \text{otherwise.} \end{cases} \quad (19)$$

Proof. Straightforward calculation. \square

Next, we introduce the necessary lemmas, propositions, and regularity assumptions that will serve as the basis for proving more specific results—both lemmas and theorems—for convex and non-convex functions.

Lemma 2 (Bounds on K_ν). *For all $t \geq 0$,*

$$0 \leq K_\nu(t) \leq \|\nu\|, \quad \text{and in particular} \quad K_\nu(0) = \|\nu\|.$$

Proof. Since $e^{-\lambda t} \in [0, 1]$ for all $\lambda \geq 0$ and $t \geq 0$, we have

$$0 \leq \int_{[0, \infty)} e^{-\lambda t} d\nu(\lambda) \leq \int_{[0, \infty)} 1 d\nu(\lambda) = \nu([0, \infty)) = \|\nu\|.$$

The identity $K_\nu(0) = \|\nu\|$ follows immediately by taking $t = 0$ in the definition of K_ν . For AdaGrad, this yields $\|\nu_{\text{AG}}\| = 1/\alpha$, and for RMSProp/Adam, $\|\nu_{\text{RM}/\text{Adam}}\| = (1 - \beta_a)/\alpha$. \square

Proposition 4 (Bounds on the Integral of K_ν). *For all $h \geq 0$,*

$$\int_0^h K_\nu(\sigma) d\sigma \leq \|\nu\| h.$$

Proof. From Lemma 2 we have $K_\nu(\sigma) \leq \|\nu\|$ for all $\sigma \geq 0$. Integrating over $[0, h]$ yields

$$\int_0^h K_\nu(\sigma) d\sigma \leq \int_0^h \|\nu\| d\sigma = \|\nu\| h.$$

\square

Lemma 3. *If ν is a finite Borel measure on $[0, \infty)$, then K_ν is completely monotone:*

$$\frac{d^k}{dt^k} K_\nu(t) = (-1)^k \int \lambda^k e^{-\lambda t} d\nu(\lambda), \quad \forall k \in \mathbb{N}.$$

In particular, it is non-increasing since $\dot{K}_\nu(t) \leq 0$ for all $t \geq 0$.

Proof. This follows directly from differentiation under the integral sign and the positivity of ν . \square

Assumption 3 (L -smoothness). *Let $f : \mathbb{R}^n \rightarrow \mathbb{R}$ be of class C^1 . There exists $L > 0$ such that*

$$\|\nabla f(x) - \nabla f(y)\| \leq L \|x - y\| \quad \forall x, y \in \mathbb{R}^n,$$

equivalently,

$$f(y) \leq f(x) + \langle \nabla f(x), y - x \rangle + \frac{L}{2} \|y - x\|^2 \quad \forall x, y \in \mathbb{R}^n.$$

To conclude the general lemmas and propositions,

Definition 2. *Throughout, the notation $M_\nu[g^2](t)$ is understood as*

$$M_\nu[\|g\|^2](t) := \int_0^t K_\nu(t - \tau) \|g(\tau)\|^2 d\tau.$$

This convention avoids ambiguities that could arise from a component-wise interpretation.

Lemma 4 (Lower bound induced by ϵ). *For all $t \geq 0$,*

$$\sqrt{M_\nu[g^2](t) + \epsilon} \geq \sqrt{\epsilon}. \quad (20)$$

Proof. Since the kernel $K_\nu(t) \geq 0$, it follows that $M_\nu[g^2](t) \geq 0$. Adding $\epsilon > 0$ to both sides yields the claimed inequality immediately. \square

With these definitions in place, we are equipped to address the convex and non-convex cases. Nevertheless, Table (1) provides a useful clarification for the reader, as it highlights the correspondence between the notation introduced in this section and that employed in the preceding one. The primary motivation for adopting this notation (in this section) is its suitability for the generalization of the theorems.

Section 3	Section 4
$G(t)$	$M_{\nu_{AG}}[g^2](t)$
$v(t)$	$M_{\nu_{RM/Adam}}[g^2](t)$
$m^i(t)$	$M_{\nu_{Adam}}^i[g](t)$

Table 1: Correspondence between the notation used in Section 3 and Section 4.

4.2 CASE I: CONVEX OBJECTIVE FUNCTIONS

In this subsection, we shall concentrate on convex objective functions, under the assumptions of regularity —Assumption 3— and convexity Bauschke & Combettes (2017).

Assumption 4 (Strong convexity). *Let $f : \mathbb{R}^n \rightarrow \mathbb{R}$ be of class C^1 . There exists $m > 0$ such that*

$$\langle \nabla f(x) - \nabla f(y), x - y \rangle \geq m \|x - y\|^2 \quad \forall x, y \in \mathbb{R}^n.$$

equivalently,

$$f(y) \geq f(x) + \langle \nabla f(x), y - x \rangle + \frac{m}{2} \|y - x\|^2 \quad \forall x, y \in \mathbb{R}^n,$$

Lemma 5. *Let $f : \mathbb{R}^n \rightarrow \mathbb{R}$ be m -strongly convex and L -smooth, with minimizer x^* . Then, for all $x \in \mathbb{R}^n$,*

$$\frac{1}{2L} \|\nabla f(x)\|^2 \leq f(x) - f(x^*) \leq \frac{1}{2m} \|\nabla f(x)\|^2.$$

Proof. **(a) Lower bound.** If f is L -smooth, then for all $x, y \in \mathbb{R}^n$,

$$f(y) \leq f(x) + \langle \nabla f(x), y - x \rangle + \frac{L}{2} \|y - x\|^2.$$

Taking $y = x^*$, the minimizer of f , we have

$$f(x^*) \leq f(x) + \langle \nabla f(x), x^* - x \rangle + \frac{L}{2} \|x - x^*\|^2,$$

or equivalently,

$$f(x) - f(x^*) \geq \langle \nabla f(x), x - x^* \rangle - \frac{L}{2} \|x - x^*\|^2.$$

By the Baillon–Haddad theorem —Bauschke & Combettes (2017), Corollary 18.16—

$$\langle \nabla f(x), x - x^* \rangle \geq \frac{1}{L} \|\nabla f(x)\|^2.$$

Moreover, by the gradient L -Lipschitz property,

$$\|\nabla f(x)\| \leq L \|x - x^*\|.$$

Substituting into the previous inequality, we deduce

$$f(x) - f(x^*) \geq \frac{1}{2L} \|\nabla f(x)\|^2.$$

(b) Upper bound. If f is m -strongly convex, then for all x, y ,

$$f(y) \geq f(x) + \langle \nabla f(x), y - x \rangle + \frac{m}{2} \|y - x\|^2.$$

Taking $y = x^*$, we get

$$f(x^*) \geq f(x) + \langle \nabla f(x), x^* - x \rangle + \frac{m}{2} \|x - x^*\|^2,$$

which is equivalent to

$$f(x) - f(x^*) \leq \langle \nabla f(x), x - x^* \rangle - \frac{m}{2} \|x - x^*\|^2.$$

Letting $g := \nabla f(x)$ and $d := x - x^*$, we maximize the quadratic form

$$\psi(d) := \langle g, d \rangle - \frac{m}{2} \|d\|^2$$

with respect to d . The maximizer is $d = g/m$, and the maximum value is

$$\max_d \psi(d) = \frac{1}{2m} \|g\|^2.$$

Therefore,

$$f(x) - f(x^*) \leq \frac{1}{2m} \|\nabla f(x)\|^2.$$

□

As the dynamics of AdaGrad and RMSProp are highly similar, differing primarily in the structure of the kernel, we may state the convergence and stability theorem in a unified form for both cases, with the sole difference arising from the Borel measure —Definition 1. Hence,

Theorem 1. *Under Assumptions 3 and 4, the solutions of*

$$\dot{\theta}^i(t) = - \frac{g^i(t)}{\sqrt{M_\nu[g^2](t + \alpha) + \epsilon}} \quad (21)$$

satisfy the bound

$$\|\theta(t) - \theta^*\| \leq \|\theta(0) - \theta^*\| e^{-m \mu_0 t}, \quad \forall t \geq 0, \quad (22)$$

where θ^* is the unique minimizer of f , $g_i(t) := \nabla_i f(\theta(t))$, $M_\nu[\cdot]$ is the memory operator with kernel K_ν defined in Definition 1, and

$$\mu_0 := \frac{1}{\sqrt{M_\nu[g^2](\alpha) + \epsilon} + \frac{\|\nu\|}{2} [f(\theta(0)) - f(\theta^*)]}.$$

Proof. Consider the function

$$\mathcal{L}(t) := \frac{1}{2} \|\theta(t) - \theta^*\|^2. \quad (23)$$

Differentiating with respect to t and using the dynamics, we obtain

$$\dot{\mathcal{L}}(t) = \langle \theta(t) - \theta^*, \dot{\theta}(t) \rangle = - \frac{\langle \theta(t) - \theta^*, g(t) \rangle}{\sqrt{M_\nu[g^2](t + \alpha) + \epsilon}}.$$

By m -strong convexity,

$$\langle \theta(t) - \theta^*, g(t) \rangle \geq m \|\theta(t) - \theta^*\|^2 = 2m \mathcal{L}(t).$$

Hence

$$\dot{\mathcal{L}}(t) \leq -2m \mu(t) \mathcal{L}(t), \quad \mu(t) := \frac{1}{\sqrt{M_\nu[g^2](t + \alpha) + \epsilon}}. \quad (24)$$

Now define $\Phi(t) := f(\theta(t)) - f(\theta^*)$. Differentiating along the flow gives

$$\dot{\Phi}(t) = \langle g(t), \dot{\theta}(t) \rangle = -\mu(t) \|g(t)\|^2.$$

Thus Φ is decreasing, since $\mu(t) > 0$ —Lemma 4—, and therefore $\Phi(t) \leq \Phi(0)$ for all $t \geq 0$. Next, define $M(t) := M_\nu[g^2](t)$. Using that $\dot{K}_\nu \leq 0$ —Lemma 3—, we obtain

$$\dot{M}(t) = \int_0^t \dot{K}_\nu(t - \tau) \|g(\tau)\|^2 d\tau + K_\nu(0) \|g(t)\|^2 \leq \|\nu\| \|g(t)\|^2,$$

where we have used $K_\nu(0) = \|\nu\|$. Consider $H(s) := \sqrt{M(s + \alpha) + \epsilon}$. Then

$$\begin{aligned} \dot{H}(s) &= \frac{\dot{M}(s + \alpha)}{2\sqrt{M(s + \alpha) + \epsilon}} \leq \frac{\|\nu\|}{2} \frac{\|g(s + \alpha)\|^2}{\sqrt{M(s + \alpha) + \epsilon}} \\ &= -\frac{\|\nu\|}{2} \frac{\sqrt{M(s + 2\alpha) + \epsilon}}{\sqrt{M(s + \alpha) + \epsilon}} \dot{\Phi}(s + \alpha) \\ &\leq -\frac{\|\nu\|}{2} \dot{\Phi}(s + \alpha). \end{aligned}$$

Integrating over $s \in [0, t]$ and using the fact that Φ is decreasing, together with Lemma 5 —namely, that $\Phi(t) \geq 0$, $\forall t > 0$ — gives

$$\sqrt{M(t + \alpha) + \epsilon} - \sqrt{M(\alpha) + \epsilon} \leq \frac{\|\nu\|}{2} (\Phi(\alpha) - \Phi(t + \alpha)) \leq \frac{\|\nu\|}{2} \Phi(0).$$

Therefore, for all $t \geq 0$,

$$\sqrt{M(t + \alpha) + \epsilon} \leq C_\nu, \quad C_\nu := \sqrt{M(\alpha) + \epsilon} + \frac{\|\nu\|}{2} \Phi(0).$$

It follows that $\mu(t) \geq \mu_0 := 1/C_\nu$. Returning to the differential inequality for $\mathcal{L}(t)$ — equation (24)— and applying Grönwall’s lemma Pachpatte (1998) (Theorem 1.2.2), we obtain

$$\mathcal{L}(t) \leq \mathcal{L}(0) \exp(-2m\mu_0 t),$$

which implies

$$\|\theta(t) - \theta^*\| \leq \|\theta(0) - \theta^*\| \exp(-m\mu_0 t).$$

This proves the claim. \square

We highlight the significance of this theorem. From equation (22), it follows that as $t \rightarrow \infty$, we have $\theta(t) \rightarrow \theta^*$, showing that the system asymptotically approaches the equilibrium point as time increases for the cases of AdaGrad and RMSProp. Furthermore, the theorem specifies the convergence rate to this minimum in the convex case, which is exponential. The rate $e^{-m\mu_0 t}$ makes explicit the cost of memory: the larger $\|\nu\|$ (i.e., a “heavier” kernel) or the larger the initialization $\Phi(0)$, the smaller μ_0 becomes and the slower the convergence.

In addition, the function in equation (23) qualifies as a Lyapunov function, as it fulfills all the necessary requirements. Consequently, this establishes the stability of the system under perturbations of the initial conditions, meaning that small deviations in the initial state do not lead to drastic changes in the solution.

While this theorem guarantees exponential convergence of $\theta(t)$ using the simple Lyapunov function, equation (23), it does not explicitly track the memory state accumulated by AdaGrad/RMSProp. Therefore, we introduce an extension of it where the memory effects are present:

Theorem 2. *Let Assumptions 3 and 4 on f hold, and consider the dynamics*

$$\dot{\theta}^i(t) = - \frac{g^i(t)}{\sqrt{M_\nu[g^2](t + \alpha) + \epsilon}},$$

where $g_i(t)$ denotes $\nabla_i f(\theta(t))$ and M_ν is the memory operator with kernel K_ν defined in Definition 1 that evolves according to the differential equation²

$$\dot{M}_\nu[g^2](t) = \lambda \|g\|^2 - \xi M_\nu[g^2](t), \quad \lambda > 0, \quad \xi \in \{0, \lambda\}.$$

Define $\Phi(t) := f(\theta(t)) - f(\theta^*)$, where θ^* is the unique minimizer of f , and consider the extended functional

$$E_\rho(t) := \Phi(t) + \rho M_\nu[g^2](t), \quad \rho > 0.$$

Then, for all $t \geq 0$, if $\mu(t) > \mu_0$ with μ_0 defined in Theorem 1 and we choose $\rho := \mu_0/(2\lambda)$, the following differential inequality holds:

$$\dot{E}_\rho(t) \leq -\kappa_0 E_\rho(t), \quad \kappa_0 := \min\{m\mu_0, \lambda\xi\} > 0,$$

and consequently,

$$E_\rho(t) \leq E_\rho(0) e^{-\kappa_0 t}, \quad \forall t \geq 0.$$

Proof. By Lemma 4, the denominator in the dynamics satisfies $\sqrt{M_\nu[g^2](t + \alpha) + \epsilon} \geq \sqrt{\epsilon}$. Reusing the argument from the proof of Theorem 1, the function $\mu(t) := 1/\sqrt{M_\nu[g^2](t + \alpha) + \epsilon}$ is uniformly bounded from below, i.e., $\mu(t) \geq \mu_0$, $\forall t \geq 0$. Differentiating Φ along trajectories,

$$\dot{\Phi}(t) = \langle g, \dot{\theta}(t) \rangle = - \frac{\|g\|^2}{\sqrt{M_\nu[g^2](t + \alpha) + \epsilon}} = -\mu(t) \|g\|^2.$$

²Indeed, this is the dynamics of M_ν employed in the proofs of Propositions 1 and 2, with $\xi = \lambda$ corresponding to the RMSProp case and $\xi = 0$ to the AdaGrad case.

Moreover,

$$\dot{M}_\nu[g^2](t) = \lambda \|g\|^2 - \xi M_\nu[g^2](t), \quad \text{with} \quad \xi \in \{0, \lambda\}. \quad (25)$$

Thus,

$$\dot{E}_\rho(t) = \dot{\Phi}(t) + \rho \dot{M}_\nu[g^2](t) = -(\mu(t) - \rho\lambda) \|g\|^2 - \rho\lambda\xi M_\nu[g^2](t). \quad (26)$$

For $t \geq 0$, $\mu(t) \geq \mu_0$. Choosing $\rho := \mu_0/(2\lambda)$ gives $\mu(t) - \rho\lambda \geq \mu_0/2$. From Lemma 5,

$$2m\Phi(t) \leq \|g\|^2 \leq 2L\Phi(t).$$

Substituting the lower bound into equation (26),

$$\dot{E}_\rho(t) \leq -\frac{\mu_0}{2} \|g\|^2 - \rho\lambda M_\nu[g^2](t) \leq -m\mu_0\Phi(t) - \lambda\rho\xi M_\nu[g^2](t).$$

Finally, setting $\kappa_0 := \min\{m\mu_0, \lambda\xi\}$, we find

$$\dot{E}_\rho(t) \leq -\kappa_0(\Phi(t) + \rho M_\nu[g^2](t)) = -\kappa_0 E_\rho(t).$$

By Grönwall's inequality Pachpatte (1998) (Theorem 1.2.2), $E_\rho(t) \leq E_\rho(0)e^{-\kappa_0 t}$, $\forall t \geq 0$, which completes the proof. \square

Once again, we emphasize this theorem. In short, E_ρ couples state and memory. When $\xi = \lambda$ (RMSProp), the forgetting term $-\xi M_\nu[g^2](t)$ (see eq. 25) yields the differential inequality $\dot{E}_\rho \leq -\kappa_0 E_\rho$ for some $\kappa_0 > 0$ —hence exponential decay. Consequently, $E_\rho(t) \rightarrow 0$ as $t \rightarrow \infty$; since $E_\rho = \Phi + \rho M_\nu[g^2]$ with $\rho > 0$ and both summands nonnegative, it follows that $\Phi(t) \rightarrow 0$ and $M_\nu[g^2](t) \rightarrow 0$ —that is, no persistent memory remains in the limit. In contrast, when $\xi = 0$ (AdaGrad), E_ρ is merely nonincreasing and the inequality does not by itself enforce an exponential rate, consistent with its cumulative memory: there is no forgetting and past contributions are not discarded.

We now turn to the case of Adam. As discussed above, this case is considered separately, since its dynamics differ slightly from the previous ones, requiring additional lemmas to prove stability and convergence. Accordingly:

Lemma 6. *If $z \geq 0$ and $z \in L^1([0, \infty))$, then*

$$\liminf_{t \rightarrow \infty} z(t) = 0.$$

In particular, there exists a sequence $t_k \rightarrow \infty$ with $z(t_k) \rightarrow 0$.

Proof. Suppose, by contradiction, that there exist $\varepsilon > 0$ and $T > 0$ such that $z(t) \geq \varepsilon$ for all $t \geq T$. Then

$$\int_0^\infty z(t) dt \geq \int_T^\infty z(t) dt \geq \int_T^\infty \varepsilon dt = \infty,$$

which contradicts the assumption $z \in L^1([0, \infty))$. Therefore, $\liminf_{t \rightarrow \infty} z(t) = 0$. The existence of a sequence $t_k \rightarrow \infty$ with $z(t_k) \rightarrow 0$ follows directly. \square

Lemma 7. *Let $M_{\nu_2}[g^2](t)$ be defined as the solution of the differential equation³*

$$\dot{M}_{\nu_2}[g^2](t) + \lambda_2 M_{\nu_2}[g^2](t) = \lambda_2 \|g\|^2, \quad \lambda_2 > 0,$$

and set

$$\mu(t) = (\sqrt{M_{\nu_2}[g^2](t)} + \varepsilon(t))^{-1}, \quad \varepsilon(t) = \varepsilon \sqrt{1 - \beta_2^{t/\alpha}}, \quad \varepsilon > 0, \quad \beta_2 \in [0, 1).$$

Then, for all $t \geq 0$,

$$\frac{\dot{\mu}(t)}{\mu(t)} = -\frac{\frac{1}{2} \frac{\dot{M}_{\nu_2}[g^2](t)}{\sqrt{M_{\nu_2}[g^2](t)}} + \dot{\varepsilon}(t)}{\sqrt{M_{\nu_2}[g^2](t)} + \varepsilon(t)}.$$

In particular,

$$\frac{\dot{\mu}(t)}{\mu(t)} \leq \frac{\lambda_2}{2}, \quad \forall t \geq 0.$$

³As noted earlier, this is precisely the same differential equation solved in Proposition 3.

Proof. Differentiating $\mu = (\sqrt{M_2} + \varepsilon)^{-1}$ gives $\dot{\mu} = -\mu^2 \left(\frac{\dot{M}_2}{2\sqrt{M_2}} + \dot{\varepsilon} \right)$. Dividing by μ yields the stated identity. Since $\dot{M}_2 \geq -\lambda_2 M_2$ and $\dot{\varepsilon} \geq 0$,

$$\frac{\dot{\mu}}{\mu} \leq -\frac{1}{2} \frac{\frac{\dot{M}_2}{\sqrt{M_2}}}{\sqrt{M_2} + \varepsilon} \leq \frac{\lambda_2}{2} \frac{\sqrt{M_2}}{\sqrt{M_2} + \varepsilon} \leq \frac{\lambda_2}{2}.$$

□

Lemma 8. Fix $\alpha > 0$ and $\beta_1, \beta_2 \in [0, 1)$. Define

$$s(t) := \frac{\sqrt{1 - \beta_2^{t/\alpha}}}{1 - \beta_1^{t/\alpha}}, \quad t \geq 0.$$

Then,

- If $\beta_1, \beta_2 \in (0, 1)$, then as $t \rightarrow 0^+$, $\frac{d}{dt} \log s(t) = -\frac{1}{2t} + O(t)$.
- If $\beta_1 = 0 \leq \beta_2 < 1$, then as $t \rightarrow 0^+$, $\frac{d}{dt} \log s(t) = \frac{1}{2t} + O(t)$.
- If $\beta_2 = 0 \leq \beta_1 < 1$, then as $t \rightarrow 0^+$, $\frac{d}{dt} \log s(t) = -\frac{1}{t} + O(t)$.
- If $\beta_1 = \beta_2 = 0$, then $\frac{d}{dt} \log s(t) \equiv 0$

Proof. We write

$$\frac{d}{dt} \log s(t) = \frac{1}{2} \frac{d}{dt} \log(1 - \beta_2^{t/\alpha}) - \frac{d}{dt} \log(1 - \beta_1^{t/\alpha}). \quad (27)$$

If $0 < \beta < 1$, set $a := -\log \beta > 0$ and $u := \frac{at}{\alpha}$. Then $\beta^{t/\alpha} = e^{-u}$ and

$$\frac{d}{dt} \log(1 - \beta^{t/\alpha}) = \frac{d}{dt} \log(1 - e^{-u}) = \frac{a}{\alpha} \frac{1}{e^u - 1}. \quad (28)$$

Applying equation (28) to β_1, β_2 and substituting into equation (27), with $a_i := -\log \beta_i > 0$ and $u_i = \frac{a_i t}{\alpha}$, we obtain

$$\frac{d}{dt} \log s(t) = \frac{1}{2\alpha} \left(\frac{a_2}{e^{u_2} - 1} - \frac{2a_1}{e^{u_1} - 1} \right), \quad (t > 0). \quad (29)$$

Using the standard expansion for $u \rightarrow 0$,

$$\frac{1}{e^u - 1} = \frac{1}{u} - \frac{1}{2} + \frac{u}{12} + O(u^3), \quad (30)$$

we find

$$\frac{a_i}{e^{u_i} - 1} = a_i \left(\frac{1}{u_i} - \frac{1}{2} + O(u_i) \right) = \frac{\alpha}{t} - \frac{a_i}{2} + O(t).$$

Substituting into equation (29):

$$\frac{d}{dt} \log s(t) = \frac{1}{2\alpha} \left[\left(\frac{\alpha}{t} - \frac{a_2}{2} + O(t) \right) - 2 \left(\frac{\alpha}{t} - \frac{2a_1}{2} + O(t) \right) \right] = -\frac{1}{2t} + \frac{2a_1 - a_2}{4\alpha} + O(t).$$

If $\beta_1 = 0 < \beta_2 < 1$, then $s(t) = \sqrt{1 - \beta_2^{t/\alpha}}$ and

$$\frac{d}{dt} \log s(t) = \frac{1}{2} \frac{d}{dt} \log(1 - \beta_2^{t/\alpha}) = \frac{1}{2} \frac{a_2}{\alpha} \frac{1}{e^{u_2} - 1}.$$

With equation (30), for $u_2 \rightarrow 0$,

$$\frac{d}{dt} \log s(t) = \frac{1}{2} \left(\frac{1}{t} - \frac{a_2}{2\alpha} + O(t) \right) = \frac{1}{2t} + O(t) \quad (t \rightarrow 0^+).$$

If $\beta_2 = 0 \leq \beta_1 < 1$, then $s(t) = (1 - \beta_1^{t/\alpha})^{-1}$ and

$$\frac{d}{dt} \log s(t) = -\frac{d}{dt} \log(1 - \beta_1^{t/\alpha}) = -\frac{a_1}{\alpha} \frac{1}{e^{u_1} - 1}.$$

Using equation (30):

$$\frac{d}{dt} \log s(t) = -\left(\frac{1}{t} - \frac{a_1}{2\alpha} + O(t)\right) = -\frac{1}{t} + O(t) \quad (t \rightarrow 0^+).$$

If $\beta_1 = \beta_2 = 0$, then $s(t) \equiv 1$ and $\frac{d}{dt} \log s(t) \equiv 0$. □

Corollary 1. *With the above definitions,*

$$\alpha(t) := s(t) \mu(t), \quad h(t) := \frac{d}{dt} \log \alpha(t) = \frac{d}{dt} \log s(t) + \frac{\dot{\mu}(t)}{\mu(t)}.$$

Then there exists $C_\alpha < \infty$ such that

$$h(t) \leq C_\alpha, \quad \forall t > 0.$$

Proof. If $\beta_1, \beta_2 \in (0, 1)$, Lemma 8 shows that $\frac{d}{dt} \log s(t) \sim -\frac{1}{2t} \rightarrow -\infty$, and Lemma 7 gives $\dot{\mu}/\mu \leq \lambda_2/2$ near 0. Hence it suffices to take

$$C_\alpha := \sup_{t \geq 0} \frac{d}{dt} \log s(t) + \lambda_2/2 < \infty.$$

If $\beta_1 = 0 < \beta_2 < 1$, then near $t = 0$ we have

$$\frac{d}{dt} \log s(t) \sim \frac{1}{2t},$$

while

$$\sqrt{M_{\nu_2}[g^2](t)} + \varepsilon(t) = \Theta(\sqrt{t}).$$

Indeed, by Taylor expansion,

$$\varepsilon(t) = \varepsilon \sqrt{1 - \beta_2^{t/\alpha}} = \varepsilon \sqrt{t} \left(\sqrt{\frac{1}{\alpha\beta_2}} \right) + O(t^{3/2}),$$

and

$$M_{\nu_2}[g^2](t) = M_{\nu_2} + \dot{M}_{\nu_2} t + O(t^2) = \lambda_2 \|g(0)\|^2 t + O(t^2),$$

where we used that $M_{\nu_2}[g^2](t)$ satisfies the differential equation

$$\dot{M}_{\nu_2}[g^2](t) + \lambda_2 M_{\nu_2}[g^2](t) = \lambda_2 \|g\|^2,$$

together with the initial condition $M_2(0) = 0$.

Hence,

$$\frac{\dot{\mu}}{\mu} = -\frac{d}{dt} \log(\sqrt{M_2(t)} + \varepsilon(t)) \sim -\frac{1}{2t}.$$

Thus the singularities cancel, and we conclude that $h(t) = O(1)$ as $t \rightarrow 0^+$. Moreover, for $t \geq \delta > 0$, both terms are continuous and bounded.

If $\beta_2 = 0 \leq \beta_1 < 1$, then $\frac{d}{dt} \log s(t) \sim -\frac{1}{t} \rightarrow -\infty$, while $\dot{\mu}/\mu \leq \lambda_2/2$, hence $h(t) \leq \lambda_2/2$ near 0 and is bounded on $[\delta, \infty)$.

In all cases, we conclude that $\sup_{t \geq 0} h(t) < \infty$. □

Theorem 3. *Let Assumptions 3 and 4 on f hold, with a unique minimizer θ^* and $g_i(t) := \nabla_i f(\theta(t))$. Consider the dynamics, for a fixed $\varepsilon > 0$,*

$$\dot{\theta}(t) = -\alpha(t) M_{\nu_1}[g](t), \quad \text{with} \quad \alpha(t) = s(t) \mu(t). \quad (31)$$

where

$$s(t) = \frac{\sqrt{1 - \beta_2^{\frac{t}{\alpha}}}}{1 - \beta_1^{\frac{t}{\alpha}}} \quad \text{with} \quad \beta_1, \beta_2 \in [0, 1) \quad \text{and} \quad \alpha \in (0, 1],$$

and

$$\mu(t) := \frac{1}{\sqrt{M_{\nu_2}[g^2](t)} + \varepsilon(t)} \quad \text{and} \quad \varepsilon(t) = \varepsilon \sqrt{1 - \beta_2^{\frac{t}{\alpha}}}.$$

(A) Dissipation and global convergence. Let $\Phi(t) := f(\theta(t)) - f(\theta^*)$ and consider the exponential kernel $K_{\nu_i}(t)$ defined in Definition 1. Define the functional

$$V(t) := \Phi(t) + \frac{\alpha(t)}{2\lambda_1} \|M_{\nu_1}[g](t)\|^2, \quad \text{with} \quad \lambda_1 = \frac{1 - \beta_1}{\alpha}, \quad (32)$$

for which, for every $t \geq 0$, and $C_\alpha < 2\lambda_1$,

$$\dot{V}(t) \leq -\alpha(t) \left[1 - \frac{C_\alpha}{2\lambda_1} \right] \|M_{\nu_1}[g](t)\|^2. \quad (33)$$

In particular, every trajectory converges to the minimizer: $\theta(t) \rightarrow \theta^*$ as $t \rightarrow \infty$.

(B) Exponential rate for Adam case. There exist constants $C, L, \omega > 0$ such that

$$\|\theta(t) - \theta^*\| \leq C e^{-\omega t}, \quad \|\nabla f(\theta(t))\| \leq L C e^{-\omega t}. \quad (34)$$

Proof. From Lemma 5, we obtain the inequality

$$\frac{1}{2L} \|\nabla f(x)\|^2 \leq f(x) - f(\theta^*) \leq \frac{1}{2m} \|\nabla f(x)\|^2. \quad (35)$$

The quantities $M_1^i(t) := M_{\nu_1}^i[g](t)$ and $M_2(t) := M_{\nu_2}[g^2](t)$ satisfy the linear ODEs

$$\dot{M}_1^i + \lambda_1 M_1^i = \lambda_1 g^i, \quad \dot{M}_2 + \lambda_2 M_2 = \lambda_2 \|g\|^2.$$

Taking the inner product of the first equation with M_1^i and using the identity $\frac{d}{dt} \|M_1\|^2 = 2\langle M_1, \dot{M}_1 \rangle$ gives

$$\langle g, M_1 \rangle = \frac{1}{2\lambda_1} \frac{d}{dt} \|M_1\|^2 + \|M_1\|^2. \quad (36)$$

Now, define $\Phi(t) = f(\theta(t)) - f(\theta^*)$ and $\alpha(t) = s(t)\mu(t)$, and set

$$V(t) = \Phi(t) + \frac{\alpha(t)}{2\lambda_1} \|M_1(t)\|^2.$$

Along the dynamics (46), we compute

$$\dot{\Phi} = \langle g, \dot{\theta} \rangle = -\alpha(t) \langle g, M_1 \rangle = -\alpha(t) \left[\frac{1}{2\lambda_1} \frac{d}{dt} \|M_1\|^2 + \|M_1\|^2 \right].$$

Differentiating V and substituting this expression yields

$$\begin{aligned} \dot{V} &= \dot{\Phi} + \frac{\dot{\alpha}}{2\lambda_1} \|M_1(t)\|^2 + \frac{\alpha(t)}{2\lambda_1} \frac{d}{dt} \|M_1(t)\|^2 \\ &= \alpha(t) \left[\frac{1}{2\lambda_1} \frac{\dot{\alpha}}{\alpha} - 1 \right] \|M_1(t)\|^2 \\ &= \alpha(t) \left[\frac{h(t)}{2\lambda_1} - 1 \right] \|M_1(t)\|^2, \end{aligned}$$

where $h(t) := \frac{d}{dt} \log \alpha(t)$; namely,

$$\dot{V}(t) \leq -\alpha(t) \left[1 - \frac{C_\alpha}{2\lambda_1} \right] \|M_1(t)\|^2, \quad (37)$$

which is strictly negative because $C_\alpha/2\lambda_1 < 1$ and $\alpha(t) > 0$ for all $t \geq 0$.

From $V(t) \leq V(0)$ and the inequality (35), we obtain

$$\|g(t)\|^2 \leq 2L\Phi(t) \leq 2LV(t) \leq 2LV(0) \quad \forall t \geq 0. \quad (38)$$

Solving the ODE for M_2 when $K_{\nu_2}(t) = \lambda_2 e^{-\lambda_2 t}$ gives

$$M_2(t) = \int_0^t \lambda_2 e^{-\lambda_2(t-s)} \|g(s)\|^2 ds \leq 2LV(0),$$

hence

$$\mu(t) \geq \frac{1}{\sqrt{2LV(0) + \varepsilon}} =: \mu^* > 0. \quad (39)$$

On the other hand, we can establish that

$$s_{\min} \leq s(t), \quad \text{with} \quad s_{\min} = \min \left\{ 1, \sqrt{\frac{\log \beta_2}{\log \beta_1}} \right\}. \quad (40)$$

Indeed, if we define

$$s(u) = \frac{\sqrt{1-y^k}}{1-y}, \quad y = e^{-a_1 u} \in (0, 1), \quad k = \frac{a_2}{a_1}, \quad a_i = -\log \beta_i, \quad u = t/\alpha,$$

we have the following cases: (a) If $k \geq 1$ (i.e., $\beta_2 \leq \beta_1$), then $y^k \leq y$, which implies $1-y^k \geq 1-y$. Hence,

$$s(u) = \frac{\sqrt{1-y^k}}{1-y} \geq \frac{\sqrt{1-y}}{1-y} = \frac{1}{\sqrt{1-y}} \geq 1.$$

(b) If $0 < k < 1$ (i.e., $\beta_2 > \beta_1$), then

$$1-y^k = \int_y^1 k t^{k-1} dt \geq k \int_y^1 dt = k(1-y).$$

Since $0 < 1-y < 1$, it follows that

$$1-y^k \geq k(1-y)^2.$$

Therefore,

$$s(u) = \frac{\sqrt{1-y^k}}{1-y} \geq \sqrt{k} = \sqrt{\frac{\log \beta_2}{\log \beta_1}},$$

when $\beta_1 = \beta_2 \neq 0$. For the case $\beta_1 = \beta_2 = 0$, we have $s(t) = 1$.

Taking into account inequalities (39) and (40), we obtain

$$\alpha(t) \geq s_{\min} \mu^* =: \alpha^*.$$

Now, integrating the differential inequality for \dot{V} —equation (37)—gives

$$\int_0^\infty \alpha(t) \|M_1(t)\|^2 dt \leq \frac{2\lambda_1}{2\lambda_1 - C_\alpha} [V(0) - V(\infty)] \leq \frac{2\lambda_1}{2\lambda_1 - C_\alpha} V(0),$$

where we have used the fact that $\dot{V}(t) \leq 0$. Therefore,

$$\int_0^\infty \|M_1(t)\|^2 dt \leq \frac{1}{\alpha^*} \int_0^\infty \alpha(t) \|M_1(t)\|^2 dt \leq \frac{2\lambda_1}{\alpha^*(2\lambda_1 - C_\alpha)} V(0) < \infty.$$

Thus, applying Lemma 6, we obtain $\|M_1(t_k)\| \rightarrow 0$ along a sequence $t_k \rightarrow \infty$. From equation (37) and the fact that $\alpha(t) > 0$, it follows immediately that

$$\dot{V}(t) = 0 \iff \|M_1(t)\| = 0.$$

Moreover, by the linear ODE $\dot{M}_1^i + \lambda_1 M_1^i = \lambda_1 g^i$ with $\lambda_1 > 0$, if $M_1^i(t) = 0$ for all $t \geq T$, then necessarily

$$0 = \lambda_1 g^i(t) \implies g^i(t) = 0, \quad t \geq T.$$

Therefore, the largest invariant set contained in $\{M_1^i = 0\}$ is precisely $\{g^i = 0\}$.

We now apply LaSalle's invariance principle Khalil (2002) (Theorem 4.4): set $\Omega := \{V \leq V(0)\}$, which is positively invariant because $V \geq 0$ and $\dot{V} \leq 0$ and (under m -strong convexity and L -smoothness, Assumptions 4 and 3) bounded, since:

1. From $\Phi \leq V(0)$ we deduce that $\|\theta(t) - \theta^*\|$ remains bounded by strong convexity:

$$\frac{m}{2} \|\theta(t) - \theta^*\| \leq \Phi(t) \leq V(t) \leq V(0).$$

2. The gradient $g_i(t) = \nabla_i f(\theta(t))$ is therefore bounded within this ball,

$$\|g(t)\| = \|\nabla f(\theta(t)) - \nabla f(\theta^*)\| \leq L \|\theta(t) - \theta^*\| \leq L V(0),$$

and by the equations of motion, both M_1^i and M_2 remain bounded as well.

With Ω compact (bounded and closed) and positively invariant, and $V \in C^1$ with $\dot{V} \leq 0$ on Ω , LaSalle applies with

$$E := \{x \in \Omega : \dot{V}(x) = 0\} = \{M_1 = 0\} \cap \Omega, \quad M := \text{largest invariant subset of } E = \{g = 0\} \cap \Omega.$$

Therefore, for any initial condition in Ω , the ω -limit⁴ set is contained in M and the trajectory approaches M as $t \rightarrow \infty$. Finally, strong convexity guarantees that $g = 0 \iff \theta = \theta^*$, and hence $\theta(t) \rightarrow \theta^*$. This establishes global convergence.

Finally, since —equation (36)—

$$\frac{d}{dt} \|M_1(t)\|^2 = 2\lambda_1 \langle M_1, g \rangle - 2\lambda_1 \|M_1\|^2,$$

the application of Young's inequality gives

$$2\lambda_1 \langle M_1, g \rangle \leq \lambda_1 \|M_1\|^2 + \lambda_1 \|g\|^2.$$

Hence,

$$\frac{d}{dt} \|M_1(t)\|^2 \leq -\lambda_1 \|M_1\|^2 + 2L\lambda_1 V, \quad (41)$$

since $\|g\|^2 \leq 2LV$. On the other hand, we already know that

$$\dot{V}(t) \leq -\alpha(t) \left(\frac{2\lambda_1 - C_\alpha}{2\lambda_1} \right) \|M_1\|^2 \leq -\alpha^* \left(\frac{2\lambda_1 - C_\alpha}{2\lambda_1} \right) \|M_1\|^2 = -\kappa \|M_1\|^2,$$

where $\kappa := \alpha^* \left(\frac{2\lambda_1 - C_\alpha}{2\lambda_1} \right)$. Thus,

$$\|M_1\|^2 \leq -\frac{1}{\kappa} \dot{V} \implies \ddot{V} \leq -\kappa \frac{d}{dt} \|M_1\|^2 \implies \ddot{V} \leq \kappa \lambda_1 \|M_1\|^2 - 2L\lambda_1 \kappa V.$$

Therefore,

$$\ddot{V} + \lambda_1 \dot{V} + 2L\lambda_1 \kappa V \leq 0.$$

This is precisely the inequality associated with a damped oscillator. Its characteristic roots are

$$r_{\pm} = \frac{-\lambda_1}{2} \pm \sqrt{\left(\frac{\lambda_1}{2}\right)^2 - 2L\kappa\lambda_1},$$

both of which have negative real part since $\lambda_1 > 0$ and $2L\kappa\lambda_1 > 0$. By the theory of linear ODEs, every solution decays exponentially. More precisely, there exists a constant $\rho := -\Re(r_+)$, such that: (a) $(\lambda_1/2)^2 \leq 2L\kappa\lambda_1$, $\rho = \lambda_1/2$, and (b) $(\lambda_1/2)^2 \geq 2L\kappa\lambda_1$, $\rho = \lambda_1/2 - \sqrt{(\lambda_1/2)^2 - 2L\kappa\lambda_1}$, therefore⁵:

$$\rho \geq \min \left\{ \frac{\lambda_1}{2}, 2\kappa L \right\},$$

and $A_1 > 0$ such that

$$V(t) \leq A_1 (|V(0)| + |\dot{V}(0)|) e^{-\rho t} = A e^{-\rho t}.$$

Next, from the inequality (41), we obtain for $C \geq \|M_1(0)\|^2 + 2L\lambda_1 A/|\lambda_1 - \rho|$

$$\|M_1(t)\|^2 \leq e^{-\lambda_1 t} \|M_1(0)\|^2 + 2L\lambda_1 A \int_0^t e^{-\lambda_1(t-s)} e^{-\rho s} ds \leq C e^{-\min(\lambda_1, \rho) t},$$

so that

$$\|M_1\| \leq \hat{C} e^{-\frac{\min(\lambda_1, \rho)}{2} t}.$$

Finally, by strong convexity we have

$$m \|\theta - \theta^*\|^2 \leq \langle g(\theta), \theta - \theta^* \rangle \leq \|g\| \|\theta - \theta^*\|.$$

⁴The ω -limit set of a trajectory $\theta(t)$ is the set of all points p for which there exists a sequence $t_k \rightarrow \infty$ with $\theta(t_k) \rightarrow p$. If the solution is bounded, the ω -limit set is nonempty, compact, and invariant, and the trajectory approaches this set as $t \rightarrow \infty$ (see, e.g., Khalil (2002)).

⁵To clarify this step: $\rho = \frac{\lambda_1}{2} - \sqrt{\left(\frac{\lambda_1}{2}\right)^2 - 2L\kappa\lambda_1} = \frac{2L\kappa\lambda_1}{\frac{\lambda_1}{2} + \sqrt{\left(\frac{\lambda_1}{2}\right)^2 - 2L\kappa\lambda_1}} \geq \frac{2L\kappa\lambda_1}{\lambda_1} = 2L\kappa$.

Therefore,

$$\begin{aligned}\|\theta(t) - \theta^*\| &\leq \frac{1}{m} \|g(t)\| \\ &\leq \frac{\sqrt{2LA}}{m} e^{-\frac{\rho}{2}t} \\ &\leq \frac{\sqrt{2LA}}{m} e^{-\frac{\min(\lambda_1, \rho)}{2}t},\end{aligned}$$

which proves the exponential rate and completes the theorem. \square

Let us emphasize this theorem once again. Under m -strong convexity and L -smoothness (Assumptions 4 and 3), the Adam-type flow admits a Lyapunov functional V —since $V > 0$, $\dot{V} \leq 0$, and $V(\theta^*) = 0$ —that guarantees global exponential stability. Moreover, both the momentums and the gradient decay exponentially,

$$M_2(t), \|M_1(t)\|^2, \|g(t)\|^2 \lesssim e^{-\rho t}, \quad \|\theta(t) - \theta^*\| \leq \hat{B} e^{-\rho t/2},$$

so that the parameters converge exponentially to the minimizer.

Another important observation is that, in the Adam case, the memory effect induced by β_2 (and its rate λ_2) is already incorporated into the constant ρ via $\kappa = \alpha^*(2\lambda_1 - C_\alpha)/2\lambda_1$ with $\alpha^* = s_{\min}\mu^*$ where

$$s_{\min} = \min\left\{1, \sqrt{\frac{\log \beta_2}{\log \beta_1}}\right\}.$$

Hence, the contribution of M_2 is already implicit in the stability constant. For this reason, the Lyapunov functional V does not explicitly include the factor M_2 : controlling V through (θ, M_1) together with μ (via M_2) is sufficient for the analysis.

4.3 CASE II: NONCONVEX OBJECTIVE FUNCTIONS

In this subsection, we work under the regularity assumption—Assumption 3—and allow functions that are not necessarily convex Nesterov (2004). The following assumption for the nonconvex analysis is:

Assumption 5 (Lower bound and precompact level set). *Let $f : \mathbb{R}^n \rightarrow \mathbb{R}$ be of class C^1 . f is bounded below, and the sublevel set*

$$\mathcal{S}_0 := \{\theta \in \mathbb{R}^n : f(\theta) \leq f(\theta(0))\}$$

is compact.

We also make use of two standard conditions (Karimi et al. (2016); Attouch et al. (2010)) for functions that need not be convex:

- **Polyak–Łojasiewicz (PL) inequality.** Let $f : \mathbb{R}^n \rightarrow \mathbb{R}$ be of class C^1 . There exists $C_{PL} > 0$ such that

$$\|\nabla f(\theta)\|^2 \geq C_{PL} [f(\theta) - f^*], \quad \text{where} \quad f^* := \inf_{\theta \in \mathbb{R}^n} f(\theta)$$

- **Kurdyka–Łojasiewicz (KL) inequality.** Let $f : \mathbb{R}^n \rightarrow \mathbb{R}$ be of class C^1 . For every critical point θ^* of f on \mathcal{S}_0 there exist $\sigma \in [0, 1)$ and $C_{KL} > 0$ such that

$$\|\nabla f(\theta)\| \geq C_{KL} [f(\theta) - f(\theta^*)]^\sigma.$$

The PL inequality is a gradient-dominance condition (assumed here to hold on the whole sublevel set \mathcal{S}_0). Under PL on \mathcal{S}_0 , any critical point in \mathcal{S}_0 has value f^* ; hence every local minimum in \mathcal{S}_0 is global. Note, however, that PL alone does not ensure existence of a critical point or attainment of f^* ; compact sublevel sets (Assumption 5) provide that. In contrast, the KL inequality is local around a given critical point: combined with a descent property and bounded sublevel sets, it guarantees convergence to some critical point, with a rate dictated by the exponent σ . As with PL, KL alone does not ensure that the limit is a minimizer; that conclusion requires convexity or PL in a neighborhood of the limit.

As in Section 4.2, before stating the main theorems we first introduce several preparatory lemmas.

Lemma 9. Consider Assumption 5 and the dynamics

$$\dot{\theta}^i(t) = - \frac{g^i(t)}{\sqrt{M_\nu[g^2](t+\alpha) + \epsilon}}, \quad (42)$$

where $g_i(t)$ denotes $\nabla_i f(\theta(t))$. Then the function $\Phi(t) := f(\theta(t)) - f(\theta^*)$ is nonincreasing, and

$$\int_0^\infty \mu(t) \|g(t)\|^2 dt = f(\theta(0)) - \lim_{t \rightarrow \infty} f(\theta(t)) < \infty.$$

Proof. Differentiating Φ along the flow yields

$$\dot{\Phi}(t) = \langle g(t), \dot{\theta}(t) \rangle = -\mu(t) \|g(t)\|^2 \leq 0,$$

where $\mu(t) = 1/\sqrt{M_\nu[g^2](t+\alpha) + \epsilon}$. Thus $\Phi(t)$ is nonincreasing. Now, integrating in time we obtain, by Assumption 5,

$$\int_0^\infty \mu(t) \|g(t)\|^2 dt = f(\theta(0)) - \lim_{t \rightarrow \infty} f(\theta(t)) \leq f(\theta(0)) - \min_{\theta \in S_0} f(\theta) < \infty,$$

which establishes the claim. \square

Lemma 10. Let $\Phi(t) = f(\theta(t)) - f(\theta^*)$ and $g_i(t) = \nabla_i f(\theta(t))$. Consider the dynamics:

$$\dot{\theta}^i(t) = - \frac{g^i(t)}{\sqrt{M_\nu[g^2](t+\alpha) + \epsilon}}. \quad (43)$$

If Φ satisfies Assumption 5, then

$$\int_0^\infty \|g(s)\|^2 ds \leq \left(\sqrt{M_\nu[g^2](\alpha) + \epsilon} + \frac{\lambda}{2} \Delta\Phi \right) \Delta\Phi, \quad \text{where } \Delta\Phi := \Phi(0) - \min_{\theta \in S_0} f(\theta).$$

Proof. Define $H(t) := \sqrt{M_\nu[g^2](t+\alpha) + \epsilon}$. For every $t \geq 0$,

$$\dot{H}(t) = \frac{1}{2} \frac{\dot{M}_\nu[g^2](t+\alpha)}{\sqrt{M_\nu[g^2](t+\alpha) + \epsilon}} = \frac{1}{2H(t)} (\lambda \|g(t+\alpha)\|^2 - \sigma M_\nu[g^2](t+\alpha)) \leq \frac{\lambda}{2H(t)} \|g(t+\alpha)\|^2,$$

where we used that $\dot{M}_\nu[g^2](t+\alpha) = -\sigma M_\nu[g^2](t+\alpha) + \lambda \|g(t+\alpha)\|^2$ with $\sigma \in \{0, \lambda\}$. On the other hand,

$$\dot{\Phi}(t) = -\mu(t) \|g(t)\|^2 \quad \text{where} \quad \mu(t) := \frac{1}{H(t)}.$$

Hence,

$$\dot{H}(t) \leq -\frac{\lambda}{2} \dot{\Phi}(t+\alpha).$$

Integrating up to T yields

$$H(T) - H(0) \leq \frac{\lambda}{2} \Delta\Phi_T, \quad \text{where} \quad \Delta\Phi_T := \Phi(\alpha) - \Phi(T+\alpha).$$

Consequently,

$$\sup_{0 \leq t \leq T} H(t) \leq H(0) + \frac{\lambda}{2} \Delta\Phi_T.$$

Therefore,

$$\int_0^T \|g(s)\|^2 ds = - \int_0^T H(s) \dot{\Phi}(s) ds \leq \sup_{0 \leq t \leq T} H(t) \Delta\Phi_T.$$

By Assumption 5, letting $T \rightarrow \infty$ gives $\Delta\Phi_T \leq \Delta\Phi$, and therefore

$$\int_0^\infty \|g(s)\|^2 ds \leq (H(0) + \frac{\lambda}{2} \Delta\Phi) \Delta\Phi.$$

\square

Lemma 11. *Under Assumptions 3 and 5, the trajectories $\theta^i(t)$ that satisfy the dynamics:*

$$\dot{\theta}^i(t) = - \frac{g^i(t)}{\sqrt{M_\nu[g^2](t + \alpha) + \epsilon}} \quad (44)$$

remain in \mathcal{S}_0 , and hence $g_i(t) = \nabla_i f(\theta(t))$ is bounded and uniformly continuous. If in addition $\int_0^\infty \|g(t)\| dt < \infty$, then $\|g(t)\| \rightarrow 0$ as $t \rightarrow \infty$.

Proof. Let $\Phi(t) = f(\theta(t)) - f(\theta^*)$. Since $\Phi(t) \leq \Phi(0)$ for all $t \geq 0$ —Lemma 9—, it follows that $\theta(t) \in \mathcal{S}_0$, which is compact by Assumption 5. By Assumption 3, ∇f is Lipschitz on \mathcal{S}_0 , and therefore uniformly continuous (Ştefan Cobzaş et al. (2019), Chapter 1.3.2). In particular,

$$\|g(t)\| \leq G_{\max}, \quad G_{\max} := \sup_{x \in \mathcal{S}_0} \|\nabla f(x)\|.$$

Thus,

$$\|\dot{\theta}(t)\| = \mu(t)\|g(t)\| \leq \frac{G_{\max}}{\sqrt{\epsilon}} =: C_\theta, \quad \text{where} \quad \mu(t) := \frac{1}{\sqrt{M_\nu[g^2](t + \alpha) + \epsilon}},$$

and integrating gives

$$\|\theta(t) - \theta(s)\| \leq \int_s^t \|\dot{\theta}(\tau)\| d\tau \leq C_\theta |t - s|,$$

so $\theta(t)$ is Lipschitz in time (hence continuous). Since ∇f is $L_{\mathcal{S}_0}$ –Lipschitz and $\theta(t) \in \mathcal{S}_0$, it follows that

$$\|g(t) - g(s)\| \leq L_{\mathcal{S}_0} \|\theta(t) - \theta(s)\| \leq L_{\mathcal{S}_0} C_\theta |t - s|,$$

which shows that g is Lipschitz in time and therefore continuous. Moreover, since $\|g(t)\| \leq G_{\max}$, the map $x \mapsto \|x\|^2$ is Lipschitz on the ball of radius G_{\max} , with constant $2G_{\max}$. Indeed,

$$\begin{aligned} \left| \|g(t)\|^2 - \|g(s)\|^2 \right| &= |\langle g(t) + g(s), g(t) - g(s) \rangle| \\ &\leq (\|g(t)\| + \|g(s)\|) \|g(t) - g(s)\| \\ &\leq 2G_{\max} \|g(t) - g(s)\|. \end{aligned}$$

Thus $\|g(t)\|^2$ is uniformly continuous. By Barbălat's lemma Farkas & Wegner (2016); Barbalat (1959), if $\|g\|^2$ is uniformly continuous and integrable —Lemma 10—, then $\|g(t)\| \rightarrow 0$ as $t \rightarrow \infty$. \square

This lemma is worth emphasizing. Notice that as $t \rightarrow \infty$ we have $\nabla f(\theta(t)) \rightarrow 0$, and therefore $\theta(t)$ approaches the set of critical points.

Theorem 4. *Assume Assumption 5. Consider the dynamics*

$$\dot{\theta}^i(t) = - \frac{g^i(t)}{\sqrt{M_\nu[g^2](t + \alpha) + \epsilon}}, \quad (45)$$

where $g_i(t)$ denotes $\nabla_i f(\theta(t))$, and note that $\theta(t) \in \mathcal{S}_0$ for all $t \geq 0$.

(PL) *If f satisfies the Polyak–Łojasiewicz inequality on \mathcal{S}_0 and there exists $\mu_0 > 0$ with $\mu(t) \geq \mu_0$ for all $t \geq 0$, then for some $\kappa > 0$,*

$$f(\theta(t)) - f^* \leq (f(\theta(0)) - f^*) e^{-\kappa t}, \quad \kappa = C_{PL} \mu_0,$$

where f^ means $\min_{\theta \in \mathcal{S}_0} f(\theta)$.*

(KL) *If f satisfies the Kurdyka–Łojasiewicz inequality on a neighborhood of $\text{Crit}(f) \cap \mathcal{S}_0$, then there exists $\theta^* \in \text{Crit}(f) \cap \mathcal{S}_0$ such that $\theta(t) \rightarrow \theta^*$ and⁶*

$$f(\theta(t)) - f^* \rightarrow 0$$

with the following rates:

⁶We write $\text{Crit}(f) := \{\theta \in \mathbb{R}^d : \nabla f(\theta) = 0\}$ for the critical set of f .

- exponential convergence if $\sigma = \frac{1}{2}$,
- polynomial rate $O(t^{-\frac{1}{1-2\sigma}})$ if $\sigma \in (\frac{1}{2}, 1)$,
- finite-time convergence if $\sigma \in [0, \frac{1}{2})$.

Proof. For the first statement, define $\Phi(t) := f(\theta(t)) - f^* > 0$, where $f^* := \min_{\theta \in S_0} f(\theta)$ exists by Assumption 5. Now, recall that $\dot{\Phi} = -\mu\|g\|^2$. Using the PL inequality, we obtain

$$\dot{\Phi}(t) \leq -\mu(t) C_{PL} \Phi(t) \leq -\kappa_{PL} \Phi(t), \quad \text{where} \quad \kappa_{PL} := \mu_0 C_{PL}.$$

Integrating yields

$$\Phi(t) \leq \Phi(T) e^{-\kappa_{PL}(t-T)}, \quad t \geq T.$$

Therefore, $\Phi(t) \rightarrow 0$ as $t \rightarrow \infty$. In particular, if the minimizer θ^* in S_0 is unique, then $\theta(t) \rightarrow \theta^*$.

For the second statement, once θ enters a neighborhood of a critical point θ^* (from some T onwards), the KL inequality gives

$$\|g(t)\| \geq C_{KL} \Phi(t)^\sigma.$$

Hence,

$$\dot{\Phi}(t) = -\mu(t)\|g(t)\|^2 \leq -\mu(t) C_{KL}^2 \Phi(t)^{2\sigma}, \quad \forall t \geq T,$$

where $\mu(t) = 1/\sqrt{M_\nu[g^2](t+\alpha) + \epsilon}$. Since $M_\nu[g^2]$ is bounded on $[0, \infty)$ —by Lemmas 2 and 10—, we have $\mu_0 := \inf_{t \geq 0} \mu(t) > 0$, and therefore

$$\dot{\Phi}(t) \leq -\kappa_{KL} \Phi(t)^{2\sigma}, \quad \text{where} \quad \kappa_{KL} := \mu_0 C_{KL}^2.$$

If $\sigma = \frac{1}{2}$, then

$$\dot{\Phi}(t) \leq -\kappa_{KL} \Phi(t) \implies \Phi(t) \leq \Phi(T) e^{-\kappa_{KL}(t-T)},$$

which yields exponential convergence. If $\sigma \in (\frac{1}{2}, 1)$, then

$$\frac{d\Phi}{\Phi^{2\sigma}} \leq -\kappa_{KL} dt.$$

Integrating from T to t gives

$$\frac{\Phi(t)^{1-2\sigma} - \Phi(T)^{1-2\sigma}}{1-2\sigma} \leq -\kappa_{KL}(t-T).$$

Since $1-2\sigma < 0$, we can rearrange to obtain

$$\Phi(t) \leq \left(\Phi(T)^{1-2\sigma} + (2\sigma-1)\kappa_{KL}(t-T) \right)^{-\frac{1}{2\sigma-1}} = O\left(t^{-\frac{1}{2\sigma-1}}\right),$$

which yields polynomial convergence. If $\sigma \in [0, \frac{1}{2})$, the same procedure applies, but now $1-2\sigma > 0$. Thus,

$$\Phi(t) \leq \left(\Phi(T)^{1-2\sigma} - (1-2\sigma)\kappa_{KL}(t-T) \right)^{-\frac{1}{2\sigma-1}} = O\left(t^{-\frac{1}{2\sigma-1}}\right).$$

Here the right-hand side reaches zero in finite time:

$$t^* = T + \frac{\Phi(T)^{1-2\sigma}}{\kappa_{KL}(1-2\sigma)},$$

so $\Phi(t) \equiv 0$ for all $t \geq t^*$. □

Under the PL inequality on the sublevel set S_0 and with an effective step bounded below ($\mu(t) \geq \mu_0 > 0$), one obtains global exponential decay of the objective gap. In particular, every critical point in S_0 has value f^* (so every local minimum in S_0 is global); if, moreover, f attains its infimum on S_0 , the trajectory $\theta(t)$ converges to the set of minimizers (and to the unique minimizer if it is isolated). By contrast, once $\theta(t)$ enters a neighborhood of the critical set, the KL inequality yields rates dictated by the exponent σ : when $\sigma = \frac{1}{2}$, the gap $f(\theta(t)) - \min_{\theta \in S_0} f(\theta)$ has exponential decay for some critical point θ^* ; for $\frac{1}{2} < \sigma < 1$ the convergence is polynomial; and if $0 \leq \sigma < \frac{1}{2}$ it vanishes in finite time. Note that KL alone does not assert that the limit is a minimizer; that conclusion requires PL in a neighborhood of the limit.

Theorem 5. Assume Assumptions 3 and 5. Let $\Phi(t) := f(\theta(t)) - f^*$, where $f^* = \min_{\theta \in \mathcal{S}_0} f$, and the functional

$$E_\rho(t) := \Phi(t) + \rho M_\nu[g^2](t).$$

Moreover, consider the dynamics

$$\dot{\theta}^i(t) = - \frac{g^i(t)}{\sqrt{M_\nu[g^2](t) + \alpha} + \varepsilon},$$

where $g_i(t)$ denotes $\nabla_i f(\theta(t))$:

- There exists $\rho^* > 0$ such that, for $\rho = \rho^*$,

$$\dot{E}_\rho(t) \leq -c_1 \|g(t)\|^2 - c_2 M_\nu[g^2](t) \leq 0,$$

for some constants $c_1, c_2 > 0$ independent of time. Consequently, E_ρ is nonincreasing.

- If f satisfies the Polyak–Łojasiewicz inequality on the sublevel set \mathcal{S}_0 , then there exists $\kappa > 0$ such that

$$E_\rho(t) \leq E_\rho(0) e^{-\kappa t}, \quad \Phi(t), M_\nu[g^2](t) \leq C e^{-\kappa t}.$$

- If f satisfies the Kurdyka–Łojasiewicz inequality on a neighborhood of $\text{Crit}(f) \cap \mathcal{S}_0$, then E_ρ and Φ admit KL rates analogous to Theorem 4.

Proof. The calculation is identical to that of Theorem 2, but without using strong convexity. Indeed, $\dot{\Phi} = -\mu \|g\|^2$ and $\dot{M}_\nu = \lambda \|g\|^2 - \xi M_\nu$, where $\xi \in \{0, \lambda\}$. Choosing $\rho = \mu_0/(2\lambda)$ with $\mu_0 \leq \mu(t)$ —as ensured by Lemmas 2 and 10 on \mathcal{S}_0 —yields

$$\dot{E}_\rho = -(\mu(t) - \rho\lambda) \|g\|^2 - \rho\lambda\xi M_\nu \leq -\frac{\mu_0}{2} \|g\|^2 - \rho\lambda\xi M_\nu,$$

which proves the first claim.

For the second, assume PL inequality holds: $\|g\|^2 \geq C_{PL} \Phi$. Then

$$\dot{E}_\rho \leq -\min\left\{\frac{\kappa_{PL}}{2}, \lambda\xi\right\} E_\rho, \quad \kappa_{PL} := \mu_0 C_{PL},$$

and integration yields the exponential decay. Finally, if KL inequality holds, $\|g\| \geq C_{KL} \Phi^\sigma$, so

$$\dot{E}_\rho \leq -\frac{\mu_0}{2} \|g\|^2 - \rho\lambda\xi M_\nu \leq -\frac{\mu_0}{2} \|g\|^2 \leq -\frac{\mu_0}{2} C_{KL}^2 \Phi^{2\sigma} \leq -\frac{\mu_0}{2} C_{KL}^2 E_\rho^{2\sigma},$$

and the KL rate estimates follow exactly as in Theorem 4. \square

Both results rely on the same memory viewpoint via E_ρ of Theorem 2. Under the PL inequality (on \mathcal{S}_0) with an effective step bounded below ($\mu(t) \geq \mu_0 > 0$), and for the case that the memory has forgetting ($\xi > 0$), one obtains exponential decay of $E_\rho(t)$, $\Phi(t)$, and $M_\nu[g^2](t)$ at rate $e^{-\kappa t}$ with $\kappa = \min\{\frac{\mu_0}{2} C_{PL}, \xi\lambda\}$ (in particular, for RMSProp, $\xi = \lambda$). Moreover, if the minimizer in \mathcal{S}_0 is unique, then $\theta(t) \rightarrow \theta^*$ as $t \rightarrow \infty$. Moreover, as in the convex case, the memory effect appears explicitly in the decay constant: stronger memory (i.e., smaller μ_0) slows down the dynamics.

With the KL condition (local around the critical set), the standard KL rates are recovered: exponential when $\sigma = \frac{1}{2}$, polynomial $t^{-\frac{1}{2\sigma-1}}$ when $\frac{1}{2} < \sigma < 1$, and finite time when $0 \leq \sigma < \frac{1}{2}$. This last phenomenon does not occur in the convex/strongly convex theorem, where the rate is always exponential.

For the case $\xi = 0$ (AdaGrad) we still have $\dot{E}_\rho \leq 0$, but the inequality cannot be closed as $\dot{E}_\rho \leq -\kappa E_\rho$. Therefore, it does not enforce an exponential rate, which is consistent with its cumulative memory, as in the convex case. Nevertheless, if $\mu(t) \geq \mu_0 > 0$ and PL holds on \mathcal{S}_0 , then $\Phi(t) \lesssim e^{-\kappa t}$ and the trajectory approaches the set of minimizers; as in the case of RMSProp, if the minimizer in \mathcal{S}_0 is unique, then $\theta(t) \rightarrow \theta^*$.

Let us point out an interesting observation that might easily be overlooked. In the convex case, strong convexity allows us to derive the convergence rate (which is exponential) directly from Φ . In contrast, in the nonconvex case this is not possible unless one imposes an additional inequality of the form $\|\theta - \theta^*\| \lesssim \Phi$, which cannot be guaranteed in general when the objective function f is not convex.⁷

⁷Or at least, the author is not aware of such a result.

Theorem 6. Assume Assumptions 5. Let $\Phi(t) := f(\theta(t)) - f^*$, where $f^* = \min_{\theta \in S_0} f(\theta)$. Consider the functional

$$V(t) = \Phi(t) + \frac{\alpha(t)}{2\lambda_1} \|M_{\nu_1}[g](t)\|^2,$$

together with the dynamics,

$$\dot{\theta}^i(t) = -\alpha(t) M_{\nu_1}^i[g](t), \quad \text{with} \quad \alpha(t) = s(t)\mu(t), \quad (46)$$

where

$$s(t) = \frac{\sqrt{1 - \beta_2^{\frac{t}{\alpha}}}}{1 - \beta_1^{\frac{t}{\alpha}}} \quad \text{with} \quad \beta_1, \beta_2 \in [0, 1), \quad \text{and} \quad \alpha \in (0, 1],$$

and

$$\mu(t) := \frac{1}{\sqrt{M_{\nu_2}[g^2](t)} + \varepsilon(t)} \quad \text{and} \quad \varepsilon(t) = \varepsilon \sqrt{1 - \beta_2^{\frac{t}{\alpha}}}.$$

Under Assumptions 3 and 5:

- If $C_\alpha/2\lambda_1 < 1$, then

$$\dot{V}(t) \leq -\alpha(t) \left[1 - \frac{C_\alpha}{2\lambda_1} \right] \|M_{\nu_1}(t)\|^2 \leq 0.$$

Moreover,

$$\int_0^\infty \alpha(t) \|M_{\nu_1}[g](t)\|^2 dt < \infty,$$

and by the linear equation $\dot{M}_{\nu_1}^i[g] + \lambda_1 M_{\nu_1}^i[g] = \lambda_1 g^i$, it follows that $\lim_{t \rightarrow \infty} \|M_{\nu_1}[g](t)\| = 0$ and $\lim_{t \rightarrow \infty} \|g(t)\| = 0$. In particular, every trajectory converges to the minimizer: $\theta(t) \rightarrow \theta^*$ as $t \rightarrow \infty$.

- If f satisfies the Polyak–Łojasiewicz inequality on the sublevel set S_0 , then there exists $\kappa > 0$ such that

$$V(t) \leq V(0) e^{-\kappa t}, \quad \Phi(t) \leq C e^{-\kappa t}.$$

- If f satisfies the Kurdyka–Łojasiewicz inequality on a neighborhood of $\text{Crit}(f) \cap S_0$, then V and Φ obey the KL rates given in Theorem 4.

Proof. Let $M_{\nu_1}^i[g](t) := M_1^i(t)$ and $M_{\nu_2}[g^2](t) := M_2(t)$. The calculation of \dot{V} is exactly as in Theorem 3, yielding the key inequality

$$\dot{V}(t) \leq -\alpha(t) \left[1 - \frac{C_\alpha}{2\lambda_1} \right] \|M_1(t)\|^2 \leq 0$$

which does not require convexity, only $C_\alpha/2\lambda_1 < 1$. Thus V is nonincreasing and, since it is bounded below by 0 (because $\Phi \geq 0$), $V(t)$ converges. Moreover, from this inequality, we get

$$\int_0^\infty \alpha(t) \|M_1(t)\|^2 dt \leq \frac{2\lambda_1}{2\lambda_1 - C_\alpha} V(0).$$

Therefore, since $\alpha(t) \geq \alpha^*$ (recall that $\alpha = s\mu$ with $s \geq s_{\min} > 0$, $\mu \geq \mu_0 > 0$, and $\alpha^* = s_{\min}\mu_0$ —proof of Theorem 3—), we obtain

$$\int_0^\infty \|M_1(t)\| dt \leq \frac{1}{\alpha^*} \frac{2\lambda_1}{2\lambda_1 - C_\alpha} V(0).$$

In particular, $\|M_1\| \in L^2(0, \infty)$, and therefore there exists a subsequence $t_k \rightarrow \infty$ such that $\|M_1(t_k)\| \rightarrow 0$ —Lemma 6—. Moreover, since M_1^i satisfies $\dot{M}_1^i + \lambda_1 M_1^i = \lambda_1 g^i$, it follows that

$$\lim_{t \rightarrow \infty} \|M_1(t)\| = 0 \quad \implies \quad \lim_{t \rightarrow \infty} \|g(t)\| = 0.$$

Since $\|g(t)\|^2$ is bounded because of Lemma 11, we obtain

$$M_{\nu_2}[g^2](t) = \int_0^t K_\nu(t-\tau) \|g(\tau)\|^2 d\tau \leq G_{\max}^2 (1 - e^{-\lambda_2 t}) \leq G_{\max}^2,$$

so that

$$\frac{1}{\sqrt{G_{\max}^2 + \epsilon}} \leq \mu(t) \leq \frac{1}{\sqrt{\epsilon}}, \quad \forall t \geq 0.$$

Similarly, $\|g(t)\|$ is bounded (again) because of Lemma 11:

$$\|M_{\nu_1}[g](t)\| \leq \int_0^t K_\nu(t-\tau) \|g(\tau)\| d\tau \leq G_{\max}.$$

Hence, the state $x(t) = (\theta, M_1, M_2)$ evolves within a compact invariant set because $\theta \in S_0$, and the ranges $0 \leq M_1^i \leq G_{\max}$ and $0 \leq M_2 \leq G_{\max}^2$ are closed and bounded intervals, and thus compact. Consider now

$$E := \{(\theta, M_1, M_2) \in \Omega : \dot{V}(\theta, M_1, M_2) = 0\} \quad \text{with} \quad \Omega := \{V \leq V(0)\}.$$

Since $\alpha(t) > 0$, we deduce $\dot{V} = 0 \iff \|M_1\| = 0$, so that $E = \{M_1^i = 0\} \cap \Omega$. Therefore, the largest invariant subset of E is $M := \{g^i = 0\} \cap \Omega$. Indeed, notice that if at some point in E we have $M_1^i = 0$ but $g^i \neq 0$, then by the differential equation for M_1^i ,

$$\dot{M}_1^i = \lambda_1 g^i \neq 0,$$

so the trajectory leaves E immediately; such points are not invariant. Therefore invariance requires

$$M_1^i = 0 \quad \text{and} \quad g^i = 0 \quad (\text{i.e., } \nabla^i f(\theta) = 0),$$

and, consequently, $M_2 = 0$. In this case the dynamics reduce to

$$\dot{\theta} = 0, \quad \dot{M}_1^i = 0, \quad \dot{M}_2 = 0,$$

which preserves $M_1 = M_2 = 0$ and θ constant. Thus $M = \{(\theta, M_1, M_2) : g = 0\} \cap \Omega$ is the largest invariant positively set. By LaSalle's invariance principle Khalil (2002) (Theorem 4.4), the ω -limit set of $x(t)$ is contained in M . In particular,

$$\lim_{t \rightarrow \infty} \|g(t)\| = 0, \quad \lim_{t \rightarrow \infty} \|M_1(t)\| = 0, \quad \lim_{t \rightarrow \infty} M_2(t) = 0,$$

which, as a consequence of $\lim_{t \rightarrow \infty} \|g(t)\| = 0$, implies that $\theta(t) \rightarrow \theta^*$.

For the last part, define

$$W(t) := \Phi(t) + \frac{\beta}{2} \|M_1(t)\|^2.$$

Differentiating and using $\dot{M}_1^i = \lambda_1(g^i - M_1^i)$, we obtain

$$\dot{W}(t) \leq (\beta\lambda_1 - \alpha(t)) \langle g(t), M_1(t) \rangle - \beta\lambda_1 \|M_1(t)\|^2.$$

Applying the inequality $\langle g, M_1 \rangle \leq |\langle g, M_1 \rangle| \leq \frac{1}{2}(\|g\|^2 + \|M_1\|^2)$ yields

$$\dot{W}(t) \leq -\left(\beta\lambda_1 - \frac{\alpha(t) - \beta\lambda_1}{2}\right) \|M_1(t)\|^2 - \frac{\alpha(t) - \beta\lambda_1}{2} \|g(t)\|^2.$$

With $\alpha(t) \geq \alpha^*$ —proof of Theorem 3—, choosing $\beta\lambda_1 = \alpha^*/2$ gives

$$\dot{W}(t) \leq -\frac{\alpha^*}{4} \|M_1(t)\|^2 - \frac{\alpha^*}{4} \|g(t)\|^2.$$

Under the PL inequality, $\|g\|^2 \geq C_{PL} \Phi$. Since $W = \Phi + \frac{\beta}{2} \|M_{\nu_1}\|^2$, we obtain

$$\dot{W} \leq -\min\left(\frac{\kappa_{PL}}{4}, \lambda_1\right) W, \quad \kappa_{PL} := \alpha^* C_{PL}.$$

Hence

$$W(t) \leq W(T) e^{-\kappa(t-T)}, \quad \kappa = \min\left(\frac{\kappa_{PL}}{4}, \lambda_1\right).$$

Therefore $\Phi(t) \leq W(t)$ also decays exponentially, and the same holds for $\|M_1(t)\|$. If KL holds, then $\|g\| \geq C_{KL} \Phi^\sigma$ for $t \geq T$, so

$$\dot{W} \leq -\frac{\mu_0}{4} C_{KL}^2 \Phi^{2\sigma} \leq -C W^{2\sigma},$$

since $W \geq \Phi$. Thus the KL rates follow as in Theorem 4, both for Φ and for M_1^i . \square

In contrast with the result based on $E_\rho = \Phi + \rho M_\nu[g^2]$, the previous theorem employs the functional $V = \Phi + \frac{\alpha}{2\lambda_1} \|M_1\|^2$, and requires only an upper bound on $h(t) := \dot{\alpha}/\alpha$, namely $C_\alpha < 2\lambda_1$, together with a positive lower bound $\alpha^* := \inf_{t \geq 0} \alpha(t) > 0$, to obtain dissipation. In particular, V is nonincreasing and $\int_0^\infty \alpha(t) \|M_1(t)\|^2 dt < \infty$, so, since $\alpha \geq \alpha^*$ and M_1^i is uniformly continuous, Barbălat's lemma Barbălat (1959) yields $\|M_1(t)\| \rightarrow 0$; using the M_1 -dynamics, this in turn implies $\|g(t)\| \rightarrow 0$, namely, $\theta(t) \rightarrow \theta^*$. Moreover, if PL (resp. KL) holds, the corresponding rates for Φ and M_1^i follow: exponential under PL; under KL, exponential when $\sigma = \frac{1}{2}$, polynomial when $\frac{1}{2} < \sigma < 1$, and finite time when $0 \leq \sigma < \frac{1}{2}$.

5 NUMERICAL SIMULATIONS

In this section, we present numerical simulations⁸ that validate the approximations proposed in the preceding sections. As shown, the simulations closely mirror the behavior of the discrete algorithms, confirming that the first-order integro-differential equations serve as accurate and reliable models for analyzing the dynamics of these optimization methods, both for convex and for nonconvex functions.

Before presenting the results, we provide an overview of the numerical method employed to solve the first-order integro-differential equations.

5.1 NUMERICAL METHOD

To solve these equations, we employed the IDESolver method as described in Gelmi & Jorquera (2014), which we implemented from scratch, tailoring it to our specific requirements rather than relying on the existing Python module. See the pseudocode in Algorithm 4. Moreover, this implementation was carried out within the JAX framework in order to fully exploit GPU-based numerical computation. The GPU used was an NVIDIA T4.

The numerical method operates as follows: It generates an initial guess for $y(x)$ by disregarding the integral term (nonlocal part) in the equation and solving the resulting ordinary differential equation. This initial guess is then used to solve the original equation, and the new solution is compared to the initial guess. The similarity between the two is quantified by an error, defined as the sum of squared differences at the discretization points:

$$\text{error} = \sum_{n=1}^M (y_{\text{current},n} - y_{\text{guess},n})^2,$$

where M denotes the total number of discretization points, $y_{\text{current},n}$ represents the current estimate of y , and $y_{\text{guess},n}$ is the guess, both evaluated at the n -th step.

If the error exceeds a predefined tolerance, a new guess y_{new} is generated by a linear combination of the current y_{current} and the old guess y_{guess} :

$$y_{\text{new}} = ay_{\text{current}} + (1 - a)y_{\text{guess}}.$$

In our implementation, the value of a is adaptive, varying based on the error between iterations, and ranges from 0.5 to 0.9999. If the error increases between iterations, a is incremented by 0.0005. This adaptation allows for finer control of convergence. We set a global error tolerance of 1×10^{-4} and a maximum number of iterations of 1×10^{10} .

For the integral calculations, we employed a Gaussian quadrature method adapted for JAX with $n = 1000$, instead of the `quad` method used in the original paper. This leads to a significant increase in calculation speed.

Additionally, we used the Euler method to solve the differential equation, rather than the RK45 method commonly employed in the original approach, to ensure consistency with Assumption 2. The (future) time increment term α of Propositions 1 and 2 is obtained using the `interp1d` interpolation function from the Interpax library.

This process continues until the error falls below the predefined tolerance. For further details on the implementation, please refer to the GitHub repository.

⁸All simulations can be reproduced from the repository available at GitHub.

Algorithm 4 Iterative Modified IDESolver Method

```
1: Initialize the iteration counter  $k \leftarrow 0$ 
2: Compute the initial solution  $y_{\text{current}}$  using the original differential equation
3: Compute the initial guess  $y_{\text{guess}}$  including the integral part with  $y_{\text{current}}$ 
4: Calculate the initial global error  $\text{error} \leftarrow \|y_{\text{current}} - y_{\text{guess}}\|$ 
5: while  $\text{error} > \text{tolerance}$  do
6:   Compute new solution  $y_{\text{new}}$  using a smoothing factor with  $y_{\text{current}}$  and  $y_{\text{guess}}$ 
7:   Update  $y_{\text{guess}}$  solving the ODE including the integral part with  $y_{\text{new}}$ 
8:   Calculate the current global error  $\text{new\_error} \leftarrow \|y_{\text{new}} - y_{\text{guess}}\|$ 
9:   if  $\text{new\_error} > \text{error}$  then
10:    if maximum smoothing factor reached then
11:      Exit the loop without achieving the desired tolerance
12:    else
13:      Update the smoothing factor to the next value
14:    end if
15:  end if
16:  Update  $y_{\text{current}} \leftarrow y_{\text{new}}$ 
17:  Increment the iteration counter  $k \leftarrow k + 1$ 
18:  if  $k > k_{\text{max}}$  then
19:    Exit the loop
20:  end if
21:  Update  $\text{error} \leftarrow \text{new\_error}$ 
22: end while
23: Set the final solution  $y \leftarrow y_{\text{guess}}$ 
24: return time values and the corresponding solution  $y$ 
```

5.2 NUMERICAL RESULTS

In this section, we present the numerical results obtained using the numerical method described previously and compare them with the outcomes derived from the original algorithms. All the figures are provided in Appendix B.

It is important to clarify that throughout this section, when we refer to “iterations,” we specifically mean the value of k as defined by the relation: $k = t/\alpha$. This should not be confused with the iterations of the numerical method used to compute the solution. The latter refers to the internal steps required to obtain the overall solution, rather than the temporal evolution of θ . To prevent confusion, we will use the term “k-iterations.”

5.2.1 CONVEX FUNCTION SIMULATIONS

We now begin with the simulations for the convex function $f(\theta) = (\theta - 4)^2$, which has a unique and well-defined minimum at $\theta^* = 4$. We begin with the nonlocal model of AdaGrad, continue with RMSProp, and conclude with Adam.

Nonlocal AdaGrad: Figure 1 shows the convergence of θ values using the nonlocal continuous AdaGrad method for minimizing the function $(\theta - 4)^2$, evaluated at two learning rates: 0.1 and 0.01. This figure demonstrates that the nonlocal continuous AdaGrad method effectively replicates the optimization dynamics of the conventional AdaGrad method.

Figure 2 depicts the evolution of the accumulated gradients $G(t)$ under the nonlocal continuous AdaGrad method. For a learning rate of 0.1, the method converges to the target value $\theta = 4$, with $G(t)$ stabilizing around 1,000 k-iterations. While this behavior closely matches the results observed with the conventional AdaGrad, a slight difference can be noted: the nonlocal continuous method reaches saturation slightly earlier than the discrete version.

When the learning rate is reduced to 0.01, the nonlocal continuous AdaGrad method still converges toward $\theta = 4$, with $G(t)$ reaching slightly above 100,000 k-iterations. As shown in Figure 2, as the learning rate decreases, the nonlocal continuous method and the discrete AdaGrad model become nearly identical, both requiring approximately 150,000 k-iterations to achieve overall stabilization.

In these simulations, AdaGrad is represented by $\xi = 0$ in Theorems 1 and 2. Theorem 1 predicts the near-exponential approach of $\theta(t)$ to the minimizer observed in Fig. 1. In turn, Theorem 2 explains the behavior of the memory: with $\xi = 0$ we only have $\dot{E}_\rho \leq -m\mu_0\Phi$, so E_ρ is nonincreasing but not forced to decay exponentially, and the accumulated squared-gradient $G(t)$ is monotone increasing and converges to a finite G_∞ , as shown in Fig. 2. Consequently, the effective step $\mu(t) = 1/\sqrt{G(t+\alpha)} + \varepsilon$ decreases and stabilizes at $1/\sqrt{G_\infty + \varepsilon}$, which explains the gradual flattening of the θ -trajectories.

Nonlocal RMSProp: Figure 3 presents the convergence trajectories for θ values using the first-order nonlocal continuous RMSProp optimizer. The figure includes two subplots corresponding to different learning rates (0.1 on the left and 0.01 on the right) and varying β parameters (0.0, 0.9, 0.99).

For θ , with a learning rate of 0.1, $\beta = 0.99$ leads to faster convergence, while $\beta = 0.0$ and $\beta = 0.9$ result in slower convergence, with the latter exhibiting more linear behavior but showing noticeable oscillations. When the learning rate is reduced to 0.01, the overall convergence slows, and the oscillatory behavior for $\beta = 0.0$ becomes less pronounced⁹.

Figure 4 shows the behavior of the squared gradients $v(t)$ under the nonlocal continuous RMSProp method. With a learning rate of 0.1, lower β values initially produce a bump followed by a decay, while higher β values exhibit a less pronounced bump. When the learning rate is decreased, this bump becomes more noticeable.

When compared to the standard RMSProp optimizer, the nonlocal continuous variant exhibits a broadly similar convergence pattern, albeit with subtle differences. For instance, for $\beta = 0.0$ and $\beta = 0.9$, the nonlocal continuous model displays a slightly different dynamic than the discrete case, attaining marginally higher values. However, as the learning rate decreases, these differences gradually vanish, and the two models become nearly indistinguishable.

Finally, these simulations are represented by $\xi = \lambda$ in Theorems 1 and 2. RMSProp has a forgetting term $-\lambda v$. The functional $E_\rho(t) = \Phi(t) + \rho v(t)$ therefore —Theorem 2— satisfies $\dot{E}_\rho \leq -\kappa_0 E_\rho$, which implies exponential decay of E_ρ , Φ and v . This is exactly what Fig. 4 shows. In the memory plots (Fig. 4), $v(t)$ decays exponentially to 0, and the decay is slower as β increases (since $\lambda = (1 - \beta)/\alpha$ is smaller). In the θ -trajectories (Fig. 3), Theorem 1 predicts the approach of $\theta(t)$ to the minimizer, as observed in Fig. 1.

Nonlocal Adam: Figures 5, 6, and 7 illustrate the behavior of the first-order nonlocal continuous Adam optimization model by showing the convergence trajectories of $\theta(t)$, $m(t)$, and $v(t)$ over time for different parameter settings (β_1 and β_2) and learning rates ($\alpha = 0.1$ and $\alpha = 0.01$).

Figure 5 shows the convergence of θ . For a higher learning rate ($\alpha = 0.1$), convergence is rapid, with different combinations of β_1 and β_2 reaching a stable value in fewer steps. However, for configurations with $\beta_1 = 0.9$, although convergence occurs more quickly, there are small oscillations, making the process slightly more unstable before reaching the minimum value. These oscillations are reduced when the learning rate is lowered to $\alpha = 0.01$. When the learning rate is lower, convergence is slower and more stable, with subtle differences in behavior between various parameter settings.

Figure 6 highlights the evolution of the first moment $m(t)$. For a learning rate of $\alpha = 0.1$, $m(t)$ demonstrates a more pronounced oscillatory behavior before stabilizing around zero. When compared to the standard Adam optimizer’s convergence of the first moment m_k , both the nonlocal and standard Adam models show identical initial oscillatory patterns. With a reduced learning rate ($\alpha = 0.01$), both models achieve smoother and more gradual convergence.

Figure 7 shows the evolution of the second moment $v(t)$. For a higher learning rate ($\alpha = 0.1$), the nonlocal continuous Adam model displays varying peak values depending on the parameter settings. Configurations such as $\beta_1 = 0.0$ and $\beta_2 = 0.99$ produce the highest peaks and the slowest decay. When compared to the standard Adam optimizer’s second moment v_k , both models follow

⁹A slight oscillation is observed for $\beta = 0.9$ and a learning rate of 0.01, induced by the numerical method, as the convergence error does not decrease below 1×10^{-4} .

similar trends, with distinct peak behaviors based on the parameter settings. Notably, the peaks for $\beta_1 = 0.0$, $\beta_2 = 0.99$ and $\beta_1 = 0.9$, $\beta_2 = 0.99$ are generally higher in the nonlocal model.

For a smaller learning rate ($\alpha = 0.01$), the model shows an increase in the size of the peaks across all parameter settings, with a more pronounced bump for $\beta_1 = 0.0$ and $\beta_2 = 0.99$ or $\beta_1 = 0.9$ and $\beta_2 = 0.99$, identical to the behavior observed in the standard case.

To conclude this section, let us analyze these plots in light of Theorem 3. Under the growth bound $C_\alpha < 2\lambda_1$ and $\alpha^* > 0$, we get $\|m(t)\| \rightarrow 0$ as $t \rightarrow \infty$. Consequently, $\|\nabla f(\theta(t))\| \rightarrow 0$, $v(t) \rightarrow 0$, and $\theta(t) \rightarrow \theta^*$. As shown, the figures confirm these theoretical predictions.

5.2.2 NONCONVEX FUNCTION SIMULATIONS

Finally, we present the simulations for the non-convex function $f(\theta) = \frac{1}{4}(\theta^2 - 1)^2$, which has different local minima at $\theta = \pm 1$ and an unstable critical point (a local maximum) at 0. In this subsection, we restrict our discussion to the case $\theta = \pm 1$, since it is of particular interest how a change in the initial conditions may lead the system to one minimum or the other. For illustrations of the case $\theta = 0$, please refer to Appendix A. All the figures are placed at Appendix B.

Before proceeding, we would like to make a brief observation regarding the position of the minima ± 1 of the nonconvex function under study. Note that they are located as mirror images of each other, so it is to be expected that the simulations will exhibit mirror symmetry when comparing the negative and positive cases, as we shall see for AdaGrad, RMSProp, and Adam.

Nonlocal AdaGrad: Figures 8a, 8b, 9a, and 9b illustrate the behavior of the nonlocal continuous AdaGrad model compared with its discrete counterpart in a nonconvex setting, for two initial conditions of θ ($\theta_0 = -0.1$ and $\theta_0 = 0.1$) and two learning rates ($\alpha = 0.1$ and $\alpha = 0.01$).

The trajectories in Figures 8a and 8b converge monotonically toward the stable minima ($\theta^* \approx -1$ and $\theta^* \approx 1$). For $\alpha = 0.1$, the nonlocal model approaches the minimum a bit more slowly than the discrete version, particularly in the early stages, although both coincide in the long run. When the learning rate is reduced to $\alpha = 0.01$, the two trajectories almost overlap, confirming the accuracy of the continuous model for smaller values of α and highlighting the system's symmetry: starting at ± 0.1 produces mirror profiles toward ± 1 , as expected.

The gradient plots in Figures 9a and 9b show a similar picture. With $\alpha = 0.1$, the nonlocal model reaches a slightly higher plateau but follows a smoother transition, while for $\alpha = 0.01$ the two curves are nearly indistinguishable across the whole time scale.

Let us discuss this figures through Lemma 11 and Theorems 4 and 5. In the figures with $\theta_0 < 0$ (Fig. 8b) and $\theta_0 > 0$ (Fig. 8a), the trajectories evolve within their respective basins and settle at limiting values. This is consistent with Lemma 11 ($\|\nabla f(\theta(t))\| \rightarrow 0$) and Theorem 4 (convergence to a critical point in \mathcal{S}_0). Furthermore, the near-exponential shape observed close to the limit is consistent with the PL case or with a KL exponent $\sigma = 1/2$. For $\xi = 0$ (Theorem 5, AdaGrad), the functional $E_\rho(t) = \Phi(t) + \rho G(t)$ is nonincreasing, but the dissipation inequality does not close as $\dot{E}_\rho \leq -\kappa E_\rho$; in particular, $G(t)$ is nondecreasing, as also occurs in the convex case. Therefore, no further decay rate for $G(t)$ is implied in this case, as illustrated in Fig. 9a or 9b.

Nonlocal RMSProp: Figures 10a, 10b, 11a, and 11b compare the first-order nonlocal continuous RMSProp model with its discrete counterpart in the nonconvex case, for two initializations $\theta_0 \in \{-0.1, 0.1\}$.

Figures 10a and 10b show monotone convergence to the stable minima $\theta^* \approx -1$ and $\theta^* \approx 1$, respectively. With the larger learning rate $\alpha = 0.1$, high momentum ($\beta = 0.99$) produces pronounced overshoots and oscillations around the target, whereas $\beta = 0$ and $\beta = 0.9$ yield smoother trajectories that stabilize more quickly. Reducing the learning rate to $\alpha = 0.01$ eliminates oscillations altogether: all settings converge smoothly, with $\beta = 0.99$ converging the fastest, followed by $\beta = 0.9$, and finally $\beta = 0$. The dynamics are symmetric with respect to the sign of the initial condition, as we discussed at the beginning of this section.

On the other hand, figures 11a and 11a report the trajectories of $v(t)$. For $\alpha = 0.1$, the nonlocal model produces smoother curves than the discrete scheme, particularly for $\beta = 0$ and $\beta = 0.99$.

When $\beta = 0$ or 0.9 , $v(t)$ exhibits a transient rise followed by decay, whereas for $\beta = 0.99$ the values remain small and relatively flat—a behavior that does not occur in the discrete case, where at $t/\alpha \approx 5$ the curve rises noticeably. With $\alpha = 0.01$, discrete and nonlocal curves nearly coincide for all β : for $\beta \in \{0, 0.9\}$, they exhibit the characteristic bell-shaped peak (largest for $\beta = 0$) before decaying to zero, while $\beta = 0.99$ keeps $v(t)$ uniformly low with a slow decrease. As in the case of $\theta(t)$, the behavior is mirrored between $\theta_0 = -0.1$ and $\theta_0 = 0.1$.

Once again, let us read the plots via Theorems 4, 5, and Lemma 11. We restrict the discussion to statements that follow directly from these results for RMSProp ($\xi = \lambda$). In the v -figures (e.g., Figs. 11a–11b), $v(t)$ decays towards 0, in line with Theorem 5; the relative speed across β agrees with the dependence of κ on λ . In the θ -panels (Figs. 10a–10b), trajectories converge to a limiting value within \mathcal{S}_0 , consistent with $\|\nabla f(\theta(t))\| \rightarrow 0$ (Lemma 11) and with the PL/KL conclusions of Theorem 4.

Nonlocal Adam: Figures 12a, 12b, 13a, and 13b, as well as 14a and 14b, compare the first-order nonlocal continuous Adam model with its discrete counterpart for both signs of the initialization $\theta_0 = \pm 0.1$ in the nonconvex setting.

Figures 12a and 12b show a rapid approach to the stable minimizers ($\theta^* \approx \pm 1$). With the larger learning rate $\alpha = 0.1$, settings with $\beta_1 = 0.9$ display overshoot and lightly damped oscillations around the limit, whereas $\beta_1 = 0$ stabilizes more quickly. The nonlocal trajectories follow the same trends (reduced oscillation amplitude) as the discrete ones. Lowering the learning rate to $\alpha = 0.01$ removes instability: all parameter choices converge smoothly and almost perfectly overlap between the nonlocal and discrete models. The dynamics are symmetric with respect to the sign of θ_0 , as discussed earlier.

In Figures 13a and 13b, $m(t)$ exhibits damped oscillations around zero for $\alpha = 0.1$, with the most pronounced swings occurring for $\beta_1 = 0.9$ (especially with $\beta_2 = 0.99$ and 0.999). For $\alpha = 0.01$, all curves show a single valley followed by a gradual decay to zero; across the whole range the nonlocal and discrete trajectories are nearly indistinguishable. As expected, the profiles for positive and negative θ_0 are mirror images.

Figures 14a and 14b show the evolution of the squared-gradient moving average $v(t)$. With $\alpha = 0.1$, the peak height and decay rate depend strongly on the parameters: $\beta_1 = 0.9, \beta_2 = 0.99$ yields the largest transient peaks, while $\beta_2 = 0.999$ (for either β_1) produces much smaller, flatter curves due to heavier averaging. For $\alpha = 0.01$, both models present the characteristic bell-shaped peak (largest for $\beta_2 = 0.99$) followed by a slow decay, and the nonlocal curves practically coincide with the discrete ones.

To conclude, let us analyze these figures via Theorem 6. What the figures show (and what the theorem certifies) is the following: (i) In the first-moment plots (Figs. 13a, 13b), one observes transient behavior that damps to $\|m(t)\| \rightarrow 0$, exactly as guaranteed by Theorem 6. (ii) In the second-moment plots (Figs. 14a, 14b), there is an initial peak followed by a decaying tail leading to $v(t) \rightarrow 0$, again in agreement with the theorem. (iii) In the θ -trajectories (Figs. 12a, 12b), the solutions stabilize at limiting values inside \mathcal{S}_0 ; this is consistent with $\|g(t)\| \rightarrow 0$.

6 CONCLUSION

In this paper, we have introduced a continuous-time formulation for the AdaGrad, RMSProp, and Adam optimization algorithms by modeling them as first-order integro-differential equations. This novel approach captures the cumulative and memory effects inherent in these adaptive methods, providing a unified and precise mathematical framework that bridges the gap between discrete algorithms and continuous dynamical systems.

Our continuous models establish a direct connection between the discrete implementations of these algorithms and their continuous counterparts. The nonlocal integral terms naturally encapsulate the algorithms' memory and adaptive behaviors, allowing the explicit representation of the influence of past gradients on current updates, Propositions 1 to 3.

Moreover, we study the convergence and stability properties of these continuous models. Theorem 1 establishes exponential convergence while revealing that memory effects slow down the rate.

Under L -smoothness and strong convexity, we construct a Lyapunov function that ensures both convergence and stability of the equilibrium point θ^* , yielding $\|\theta(t) - \theta^*\| \leq \|\theta(0) - \theta^*\| e^{-m\mu_0 t}$, with an explicit decay constant μ_0 that decreases with both the memory magnitude $\|\nu\|$ and the initial optimization gap. The distinction between AdaGrad and RMSProp arises naturally through the parameter ν .

To separate accumulation from forgetting, Theorem 2 introduces the functional $E_\rho = \Phi + \rho M_\nu[g^2]$ and proves a closed dissipation inequality $\dot{E}_\rho \leq -\kappa_0 E_\rho$, where $\kappa_0 = \min\{m\mu_0, \lambda\xi\}$. The memory obeys $\dot{M}_\nu[g^2] = -\xi M_\nu[g^2] + g^2$, so $-\xi M_\nu[g^2]$ acts as forgetting and g^2 acts as accumulation. Hence RMSProp ($\xi = \lambda$) yields exponential decay of E_ρ , both the memory and the objective gap via κ_0 , whereas AdaGrad ($\xi = 0$) is a pure accumulator, $\dot{E} = 0$, ensuring monotone descent—via Theorem 1—but no exponential rate. Regarding the rate, $m\mu_0$ decreases as the memory magnitude $\|\nu\|$ grows (more memory implies smaller μ_0), while $\lambda\xi$ increases with λ . Consequently, κ_0 increases with weaker memory (smaller $\|\nu\|$) up to the ceiling $m\mu_0$, but decreases with stronger memory (larger $\|\nu\|$). In particular, for AdaGrad $\kappa_0 = \min\{m\mu_0, 0\} = 0$, hence no exponential rate.

For Adam, Theorem 3 establishes both convergence and stability through the Lyapunov functional $V = \Phi + \frac{\alpha}{2\lambda_1} \|M_{\nu_1}[g]\|^2$. Stability follows from the Lyapunov framework itself, while convergence arises under the assumptions $h(t) = \frac{d}{dt} \log \alpha(t) \leq C_\alpha < 2\lambda_1$ and $\alpha(t) \geq \alpha^* > 0$. By applying LaSalle’s invariance principle to V , we obtain global convergence, namely $\theta(t) \rightarrow \theta^*$ and $\|M_{\nu_1}[g](t)\| \rightarrow 0$. Once convergence is guaranteed, using an inequality of the damped oscillator of V , we obtain exponential convergence to the minimizer θ^* .

The nonconvex analysis mirrors this picture. Lemma 11 ensures that, for AdaGrad and RMSProp, we have $\theta(t) \rightarrow \theta^*$ as $t \rightarrow \infty$ by an application of Barbălat’s lemma, since $\nabla f(t) \rightarrow 0$ in the limit. Building on Lemma 11, Theorem 4 guarantees exponential decay under the Polyak–Łojasiewicz (PL) condition, and finite, polynomial or exponential convergence under the more general Kurdyka–Łojasiewicz (KL) framework. Specifically, if the KL exponent satisfies $\theta \in (0, 1/2)$, convergence occurs in finite time, whereas for $\sigma = 1/2$ it becomes exponential.

Finally, when $\sigma \in (1/2, 1)$, the rate transitions to a polynomial regime, $O(t^{-\frac{1}{1-2\sigma}})$, all of which hold locally, in a neighborhood of the stationary point. Following the same reasoning and using the same functionals as in Theorems 2 and 3, Theorems 5 and 6 extend the energy functionals E_ρ (for AdaGrad/RMSProp) and V (for Adam) to the nonconvex setting. These results ensure that $\theta(t)$ stabilizes toward the critical set—via LaSalle’s invariance principle in Theorem 6—and that exponential convergence holds under the PL condition, while KL-type local rates govern the general nonconvex case. In this regime, both the gradient norms and Adam’s momentum terms vanish asymptotically within the attraction basin of a local minimizer θ^* , assuming such a minimizer exists. However, these results do not assert the uniqueness of the limit point, as multiple local minima may coexist.

Through extensive numerical simulations, we have demonstrated that these continuous formulations accurately reproduce the convergence dynamics and behaviors of the original algorithms across a wide range of settings, including different learning rates and parameter configurations. Furthermore, as the learning rate decreases, the similarity between the continuous and discrete models increases, confirming the effectiveness of the continuous representation in capturing the behavior of the discrete algorithms. The simulations also align closely with the theoretical predictions: in AdaGrad, trajectories approach minimizers in the convex case (critical points in the nonconvex case) while the accumulated memory saturates and the effective step shrinks, flattening the curves; in RMSProp, the memory decay exponentially, with slower rates as the memory becomes stronger ($\beta \rightarrow 1$); and in Adam, both moments damp and the parameters stabilize, with longer transients under stronger memory.

However, while our continuous-time models provide valuable insights, they are based on deterministic settings and simplified objective functions. Extending these models to handle stochasticity, high-dimensional parameter spaces, and the complex architectures of modern neural networks is a natural next step. Furthermore, addressing the computational complexity associated with solving integro-differential equations is essential for enhancing their practical applicability, highlighting the need for efficient computational strategies.

In conclusion, our findings suggest that the integro-differential approach not only provides a valid method for representing the dynamics of AdaGrad, RMSProp, and Adam in a continuous-time framework but also serves as a powerful tool for advancing the theoretical understanding of these widely used optimization algorithms. By bridging discrete and continuous optimization methods, this approach has the potential to inspire novel methodologies and applications in AI research that involve memory (nonlocal) effects. Such applications include nonlocal Lagrangian or Hamiltonian formalisms and the extension of Noether’s Theorem for nonlocal Lagrangians, which we could further explore in future work Heredia & Llosa (2021); Heredia (2023).

ACKNOWLEDGMENTS

I would like to express sincere gratitude to Josep Llosa (University of Barcelona), Rhys Gould (University of Cambridge), Hidenori Tanaka (Harvard University), and Javier Cristin (Autonomous University of Barcelona) for their insightful discussions on nonlocality and valuable feedback on this manuscript. I also thank the Digital Transformation Team and the Nennisiwok Team at DAMM for their ongoing support.

AUTHOR CONTRIBUTIONS

Carlos Heredia was solely responsible for the conception, development, implementation, and writing of this manuscript.

FUNDING

The author declares that no funding was received for this work.

A NONCONVEX SIMULATION. CASE $\theta^* = 0$.

This section illustrates the simulations for the $\theta^* = 0$ case of the nonconvex function $\frac{1}{4}(\theta^2 - 1)^2$. Note that this case is trivial: since the initial condition is $\theta_0 = 0$, the system starts at the critical (maximum) point and therefore remains there, as shown in Fig. 15. As can be observed in the non-convex plots, any small perturbation causes the system to converge to one of the local minima.

On the other hand, since all the plots for AdaGrad, RMSProp, and Adam are identical, with all trajectories remaining at the minimum $\theta_0 = 0$, we only display the first one: AdaGrad. The others can be found in the `simulations/figures` folder of the GitHub repository.

B SIMULATION FIGURES

In this section, we present the simulation figures for both the convex and nonconvex cases.

B.1 CONVEX CASES

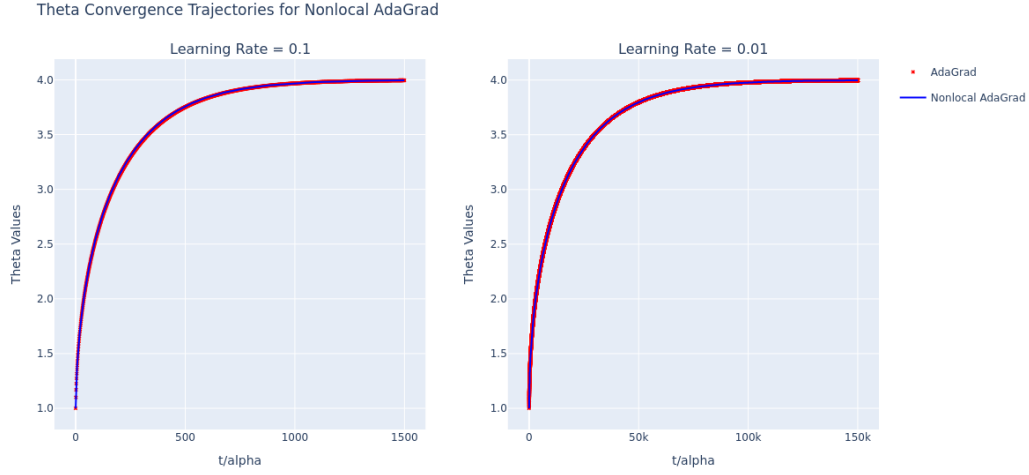


Figure 1: **Convergence of $\theta(t)$ using the first-order nonlocal continuous AdaGrad method.** The plot illustrates the convergence trajectories for minimizing the function $(\theta - 4)^2$ using two different learning rates: 0.1 (left) and 0.01 (right). At a higher learning rate (0.1), the algorithm rapidly converges to the target value $\theta = 4$, stabilizing in under 1,500 k-iterations. With a lower learning rate (0.01), the convergence is more gradual, reaching the target around 100,000 k-iterations.

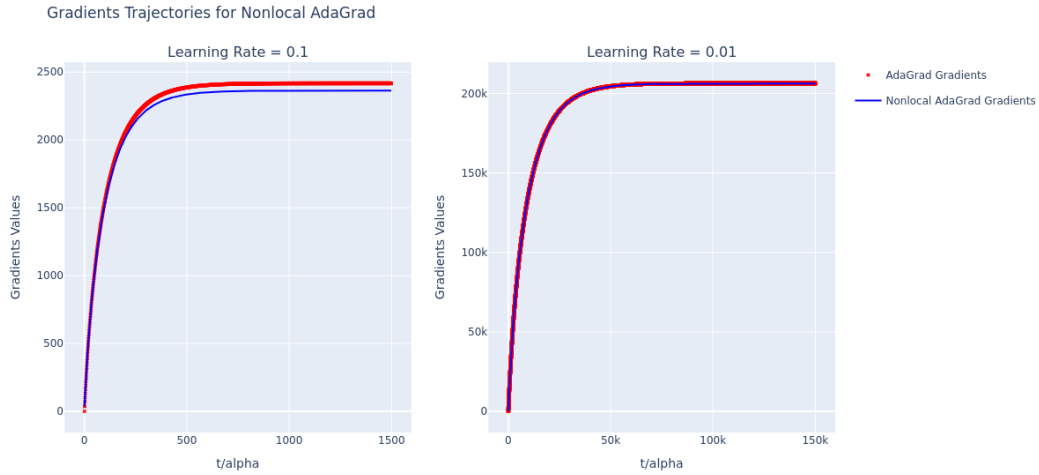


Figure 2: **Accumulated gradients $G(t)$ convergence trajectories using the first-order nonlocal continuous AdaGrad method.** The plot shows that the nonlocal continuous AdaGrad method exhibits a nearly identical gradient accumulation behavior to the conventional AdaGrad method, with rapid convergence and stabilization at both learning rates.

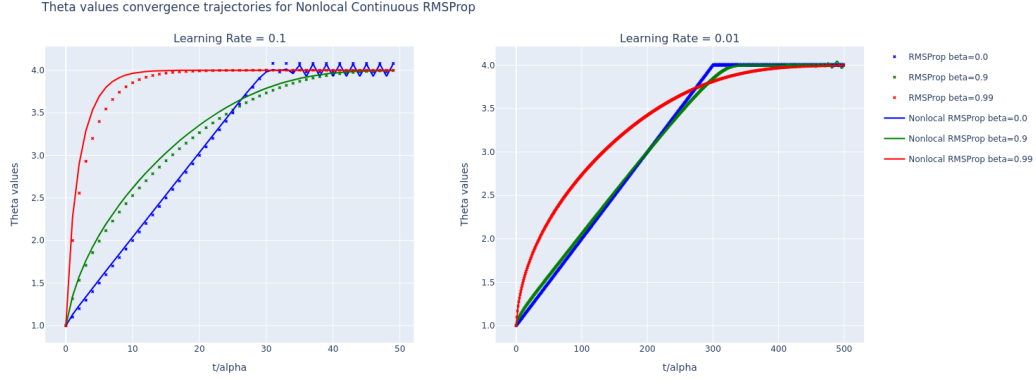


Figure 3: **Convergence of $\theta(t)$ using the first-order nonlocal continuous RMSProp method.** The plot shows the convergence to the minimum value of $\theta = 4$ for the convex function $(\theta - 4)^2$. The left subplot corresponds to a learning rate of 0.1, while the right subplot uses a learning rate of 0.01. With a learning rate of 0.1, $\beta = 0.0$ exhibits more noticeable oscillations, whereas $\beta = 0.9$ and 0.99 converge more smoothly. For a learning rate of 0.01, a slight destabilization occurs for $\beta = 0.9$ as the solution approaches the final result, caused by the numerical method. At higher learning rates, slight differences can be observed between the models: for $\beta = 0.0$, the oscillations in the discrete case start immediately upon reaching the minimum, whereas in the continuous case, they take a few k -iterations to begin. On the other hand, for $\beta = 0.99$, the curve is less pronounced in the discrete model compared to the continuous one.

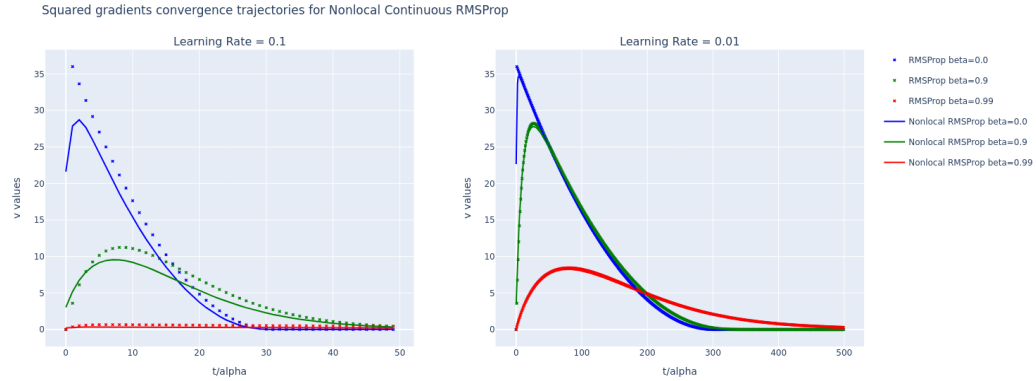


Figure 4: **Convergence trajectories of $v(t)$ for the first-order nonlocal continuous RMSProp method.** This plot illustrates the convergence of the squared gradient moving average $v(t)$. The left subplot represents a learning rate of 0.1, while the right subplot corresponds to a learning rate of 0.01. For β values of 0.0 and 0.9, a slight initial bump is noticeable, but both eventually decay towards zero. The main differences between the continuous and discrete models appear at a learning rate of 0.1, where the values are slightly higher for $\beta = 0.9$ and $\beta = 0.99$, and for $\beta = 0.0$ a small bump is observed instead of a direct descent.

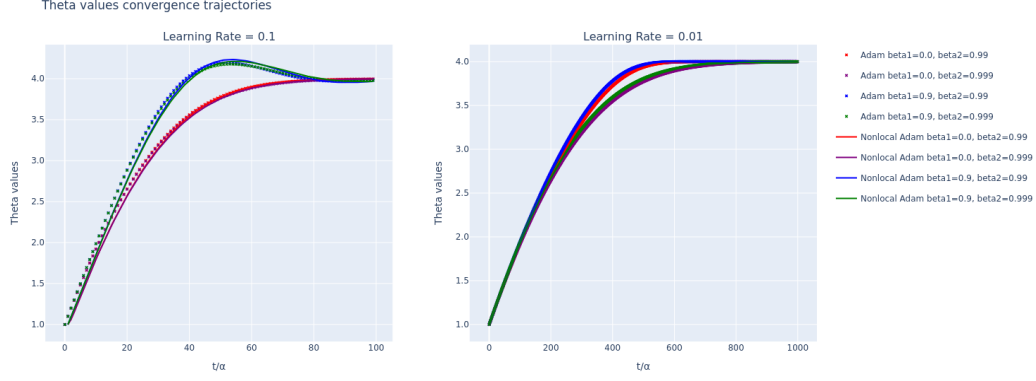


Figure 5: **Convergence of $\theta(t)$ using the first-order nonlocal continuous Adam method.** The plot illustrates the convergence trajectories of θ -values for the first-order nonlocal continuous Adam model under different parameter settings of β_1 and β_2 with two distinct learning rates (0.1 and 0.01). For $\beta_1 = 0.9$ and a learning rate of 0.1, a noticeable oscillation is observed, requiring a longer time to stabilize at the minimum value. This behavior improves when the learning rate is reduced to 0.01.

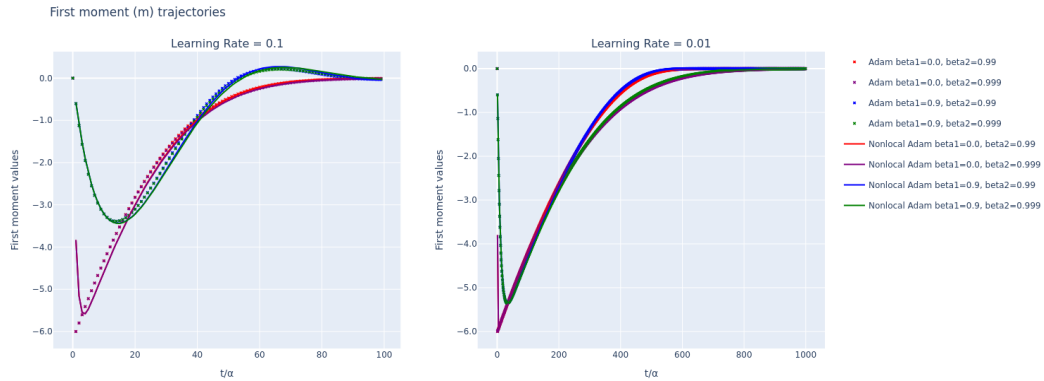


Figure 6: **Convergence trajectories of $m(t)$ for the first-order nonlocal continuous Adam optimizer.** The plot shows the evolution of the first moment $m(t)$ over time, scaled by the learning rate. With a higher learning rate ($\alpha = 0.1$), the values of $m(t)$ exhibit certain oscillations, whereas a lower learning rate ($\alpha = 0.01$) results in a smoother and slower convergence.

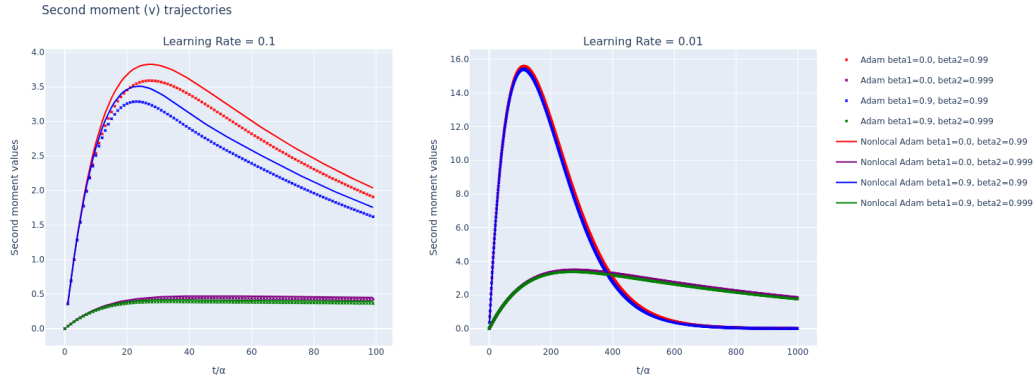
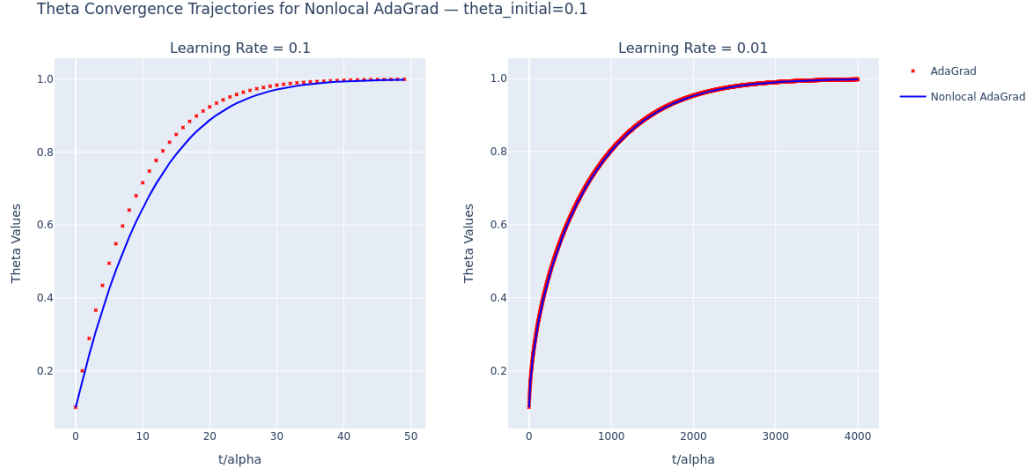
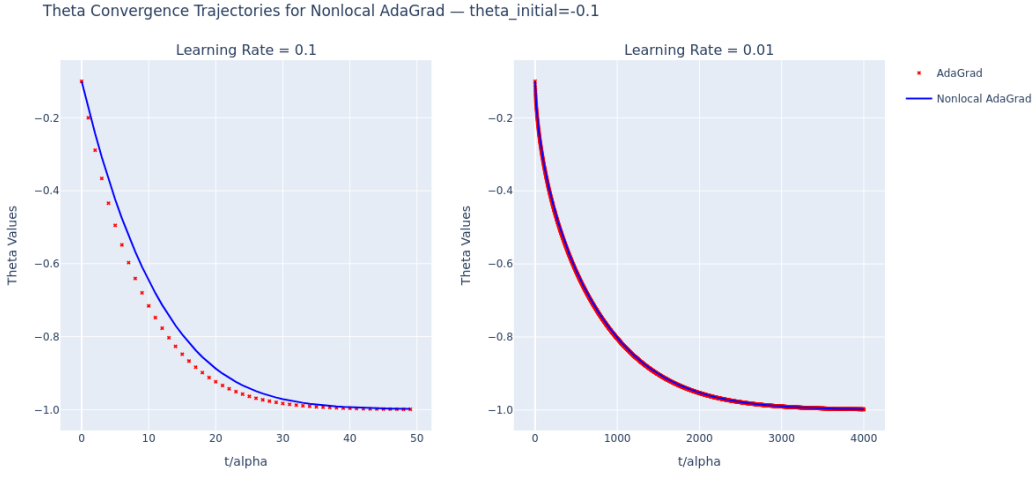


Figure 7: **Convergence trajectories of $v(t)$ for the first-order nonlocal continuous Adam optimizer.** The plot illustrates the convergence of the squared gradient moving average $v(t)$. At a higher learning rate ($\alpha = 0.1$), the peaks of $v(t)$ vary according to the parameter settings, with $\beta_1 = 0.0$ and $\beta_2 = 0.99$ producing the most significant peak and the slowest rate of decay. When the learning rate is reduced to 0.01, all curves display a more pronounced initial peak followed by a gradual decline.

B.2 NONCONVEX CASES

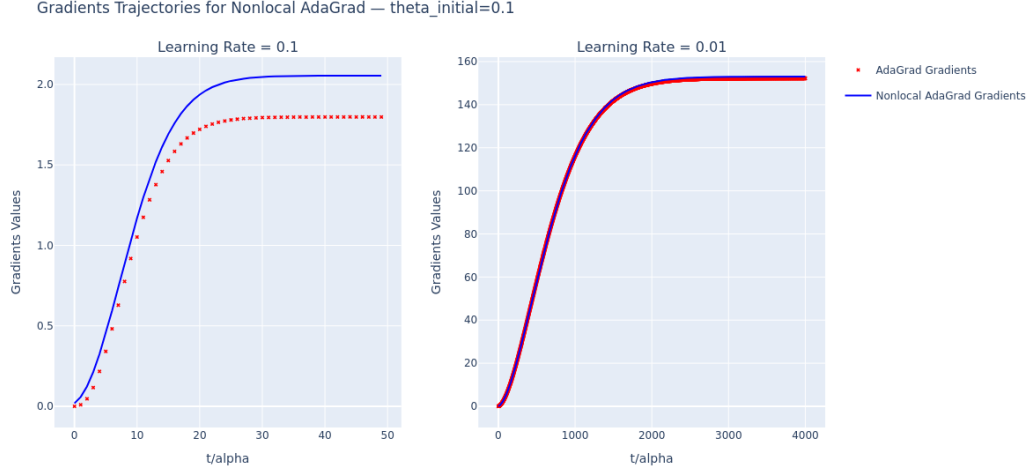


(a) **Convergence of $\theta(t)$ with $\theta_0 = 0.1$ for AdaGrad.** The nonlocal method and discrete AdaGrad converge monotonically towards $\theta^* \approx 1$. With $\alpha = 0.1$, the nonlocal approximation is slightly smoother; with $\alpha = 0.01$, both trajectories overlap almost completely, although they require many more iterations.

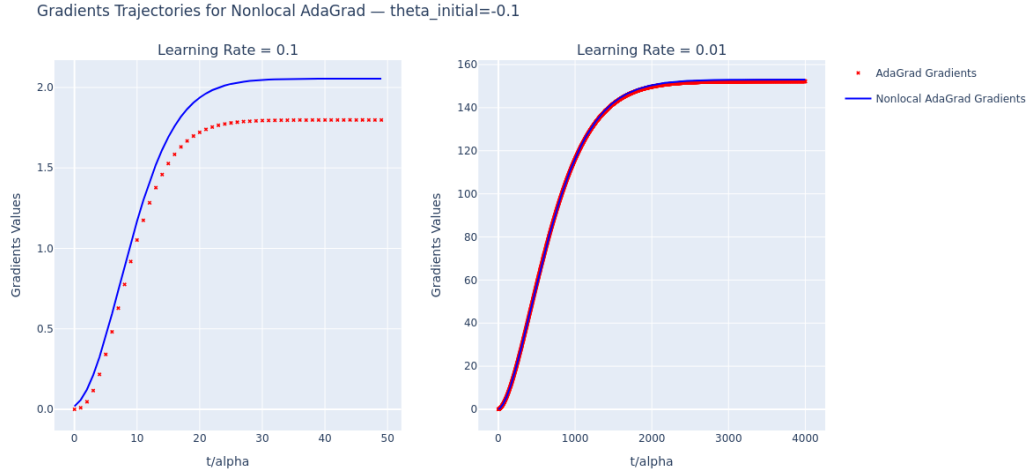


(b) **Convergence of $\theta(t)$ with $\theta_0 = -0.1$ for AdaGrad.** Symmetric behavior with respect to the positive case: monotonic convergence to $\theta^* \approx -1$. At $\alpha = 0.1$, the nonlocal model is slightly slower at the beginning; at $\alpha = 0.01$, both curves essentially coincide throughout the entire interval.

Figure 8: **AdaGrad numerical simulations.** These two plots show the evolution of the trajectory of $\theta(t)$ for the nonconvex function $\frac{1}{4}(\theta^2 - 1)^2$ with two initial conditions $\theta_0 = \pm 0.1$ for AdaGrad.

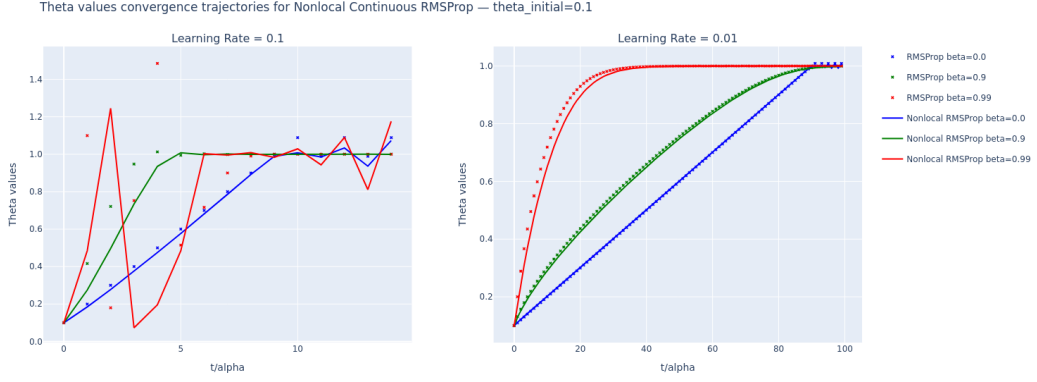


(a) **Gradient trajectories for nonlocal and discrete AdaGrad dynamics with initial value $\theta_0 = 0.1$.** Gradient trajectories with $\theta_0 = 0.1$. For $\alpha = 0.1$, the nonlocal model reaches a slightly higher plateau and shows a smoother transition than discrete AdaGrad; for $\alpha = 0.01$, both trajectories overlap almost completely throughout t/α .

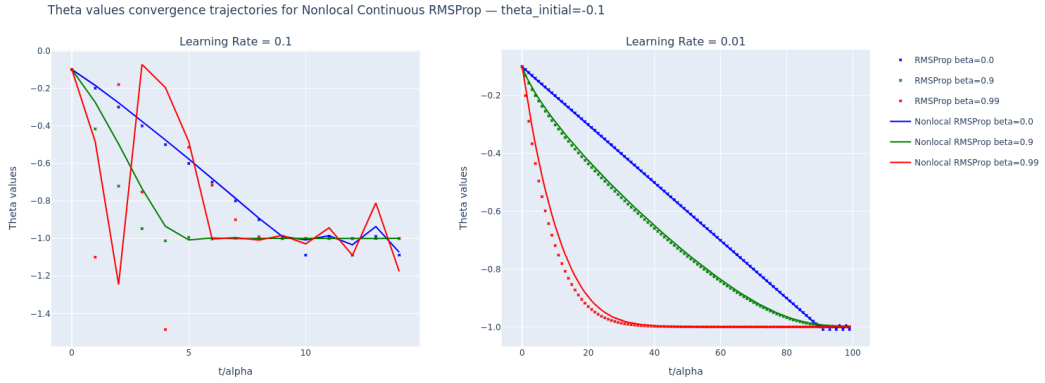


(b) **Gradient trajectories for nonlocal and discrete AdaGrad dynamics with initial value $\theta_0 = -0.1$.** Gradient trajectories with $\theta_0 = -0.1$. Results analogous to the case $\theta_0 = 0.1$: at $\alpha = 0.1$ the nonlocal term is smoother and reaches a slightly higher plateau; at $\alpha = 0.01$ the agreement with the discrete scheme is practically exact.

Figure 9: **Gradient trajectories of AdaGrad.** These two plots show the evolution of the trajectory of the gradient $G(t)$ for the nonconvex function $\frac{1}{4}(\theta^2 - 1)^2$ with two initial conditions $\theta_0 = \pm 0.1$ for AdaGrad.

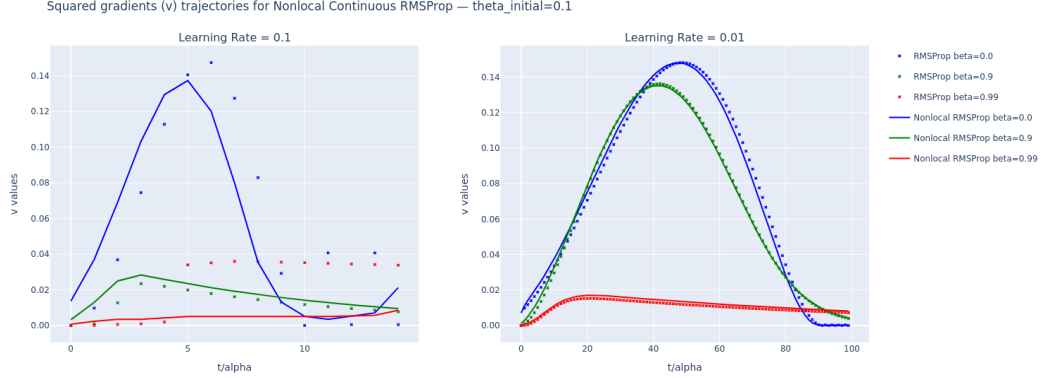


(a) **Convergence trajectories of $\theta(t)$ with $\theta_0 = 0.1$ for the nonlocal and discrete models.** At $\alpha = 0.1$, high momentum ($\beta = 0.99$) leads to pronounced overshoot/oscillations; $\beta = 0$ and 0.9 are smoother. At $\alpha = 0.01$, all settings converge smoothly with ordering of speeds $\beta = 0.99 > 0.9 > 0$. Nonlocal and discrete trajectories closely agree, especially for the smaller learning rate.

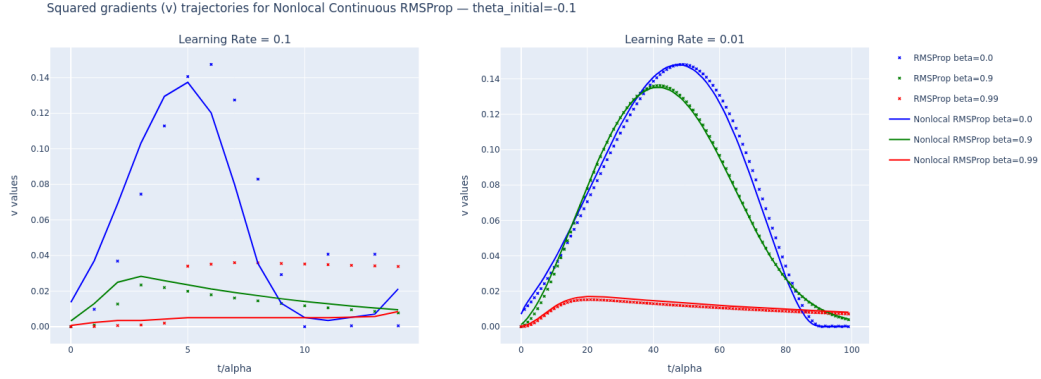


(b) **Convergence trajectories of $\theta(t)$ with $\theta_0 = -0.1$ for the nonlocal and discrete models.** Mirror behavior of the positive case: convergence to $\theta^* \approx -1$ with oscillations for $\beta = 0.99$ when $\alpha = 0.1$, and smooth, rate-ordered convergence for $\alpha = 0.01$.

Figure 10: **Convergence trajectories of $\theta(t)$ for the nonlocal and discrete RMSProp models.** These two plots show the evolution of the trajectory of $\theta(t)$ for the nonconvex function $\frac{1}{4}(\theta^2 - 1)^2$ with two initial conditions $\theta_0 = \pm 0.1$ for RMSProp.

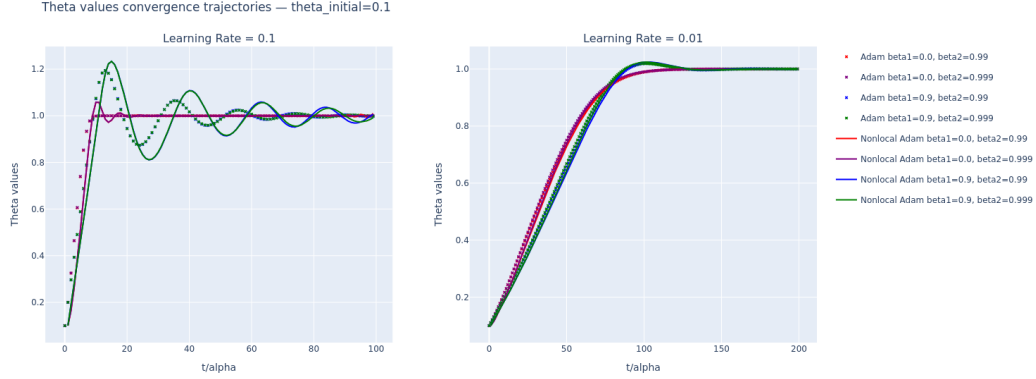


(a) **Squared-gradient trajectories of $v(t)$ for the nonlocal and discrete momentum models with positive initialization.** Squared-gradient trajectories $v(t)$ with $\theta_0 = 0.1$. For $\alpha = 0.1$, nonlocal curves are smoother than the discrete ones; $\beta = 0, 0.9$ display a transient peak then decay, while $\beta = 0.99$ stays small and nearly flat. For $\alpha = 0.01$, discrete and nonlocal curves almost overlap: $\beta \in \{0, 0.9\}$ show a bell-shaped peak (larger for $\beta = 0$) followed by decay, and $\beta = 0.99$ remains low throughout.

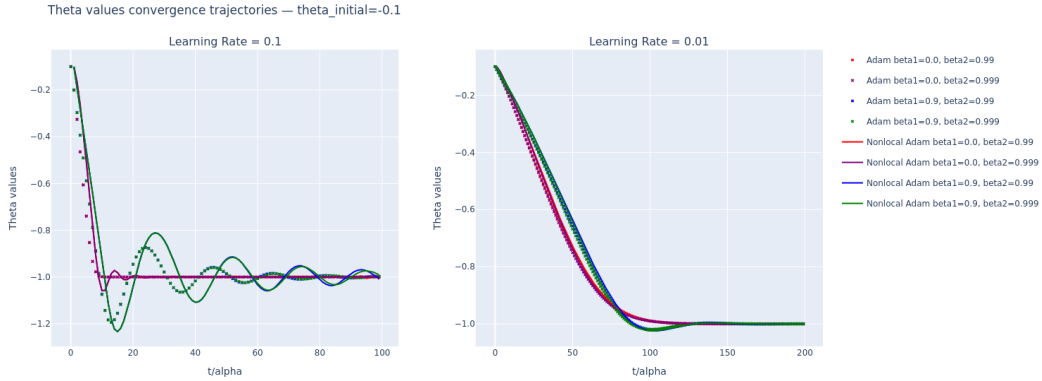


(b) **Squared-gradient trajectories of $v(t)$ for the nonlocal and discrete momentum models with negative initialization.** Squared-gradient trajectories $v(t)$ with $\theta_0 = -0.1$. Same qualitative pattern as for $\theta_0 = 0.1$: nonlocal curves are smoother at $\alpha = 0.1$; with $\alpha = 0.01$ both models align closely, with the largest peaks for $\beta = 0$, smaller for $\beta = 0.9$, and consistently low values for $\beta = 0.99$.

Figure 11: Squared-gradient trajectories of $v(t)$ for the nonlocal and discrete RMSProp models. These two plots show the evolution of the trajectory of the gradient $v(t)$ for the nonconvex function $\frac{1}{4}(\theta^2 - 1)^2$ with two initial conditions $\theta_0 = \pm 0.1$ for RMSProp.

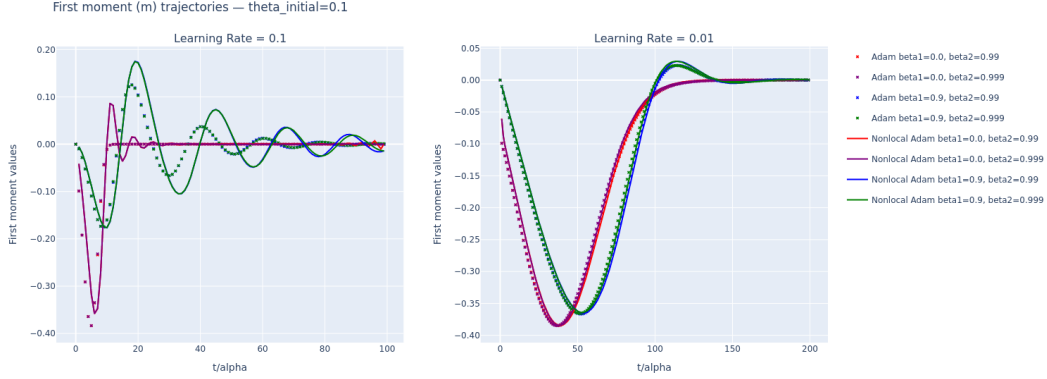


(a) **Convergence trajectories of $\theta(t)$ for the nonlocal and discrete Adam models with positive initialization.** Convergence of $\theta(t)$ with $\theta_0 = 0.1$. Solid lines: first-order nonlocal continuous Adam; markers: discrete Adam. Two learning rates ($\alpha = 0.1, 0.01$) and parameters $\beta_1 \in \{0, 0.9\}$, $\beta_2 \in \{0.99, 0.999\}$ are considered. With $\alpha = 0.1$, the $\beta_1 = 0.9$ configurations exhibit overshooting and lightly damped oscillations, whereas with $\alpha = 0.01$ all curves converge smoothly and nearly overlap, approaching $\theta^* \approx 1$.

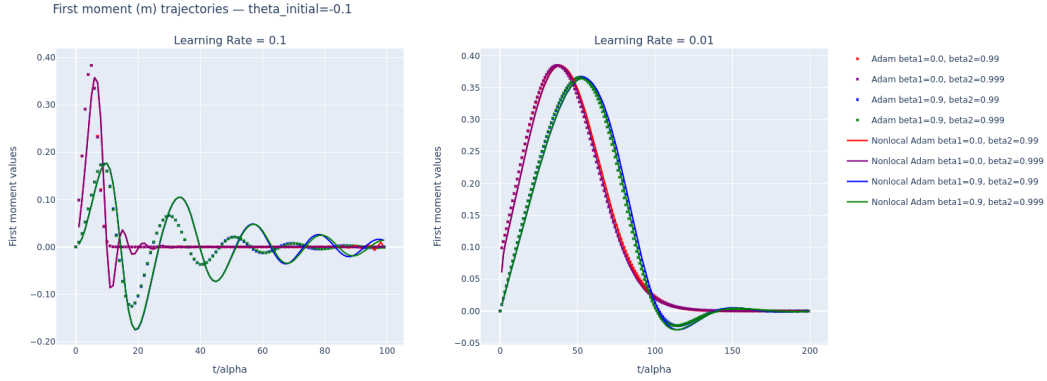


(b) **Convergence trajectories of $\theta(t)$ for the nonlocal and discrete Adam models with negative initialization.** Convergence of $\theta(t)$ with $\theta_0 = -0.1$. Same setup as Fig. 12a. For $\alpha = 0.1$, $\beta_1 = 0.9$ produces mild oscillations; for $\alpha = 0.01$ the trajectories are smooth and almost identical between the nonlocal and discrete models, converging to $\theta^* \approx -1$.

Figure 12: **Convergence trajectories of $\theta(t)$ for the nonlocal and discrete Adam models.** These two plots show the evolution of the trajectory of $\theta(t)$ for the nonconvex function $\frac{1}{4}(\theta^2 - 1)^2$ with two initial conditions $\theta_0 = \pm 0.1$ for Adam.

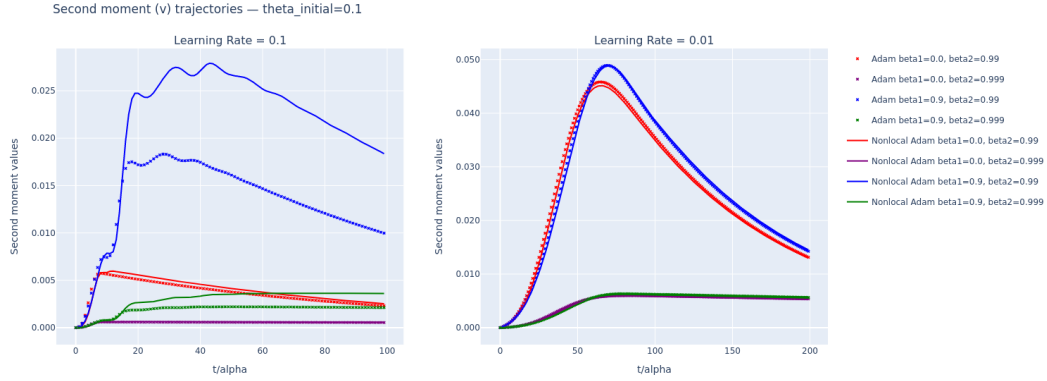


(a) **First-moment trajectories of $m(t)$ for the nonlocal and discrete Adam models with positive initialization.** First-moment trajectories $m(t)$ with $\theta_0 = 0.1$. At the larger learning rate $\alpha = 0.1$, $m(t)$ exhibits damped oscillations around zero—most pronounced for $\beta_1 = 0.9$ and $\beta_2 = 0.999$. With $\alpha = 0.01$, all curves show a single hump followed by decay to zero. Nonlocal and discrete results closely match across regimes.

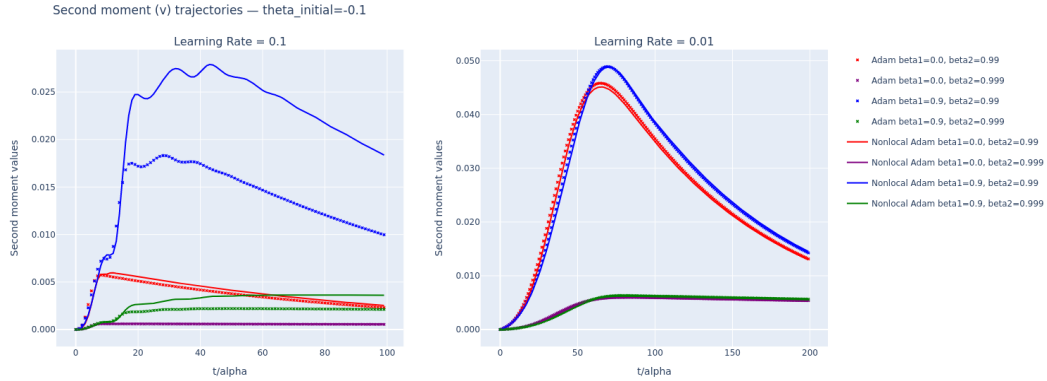


(b) **First-moment trajectories of $m(t)$ for the nonlocal and discrete Adam models with negative initialization.** First-moment trajectories $m(t)$ with $\theta_0 = -0.1$. Mirror behavior of the positive case. For $\alpha = 0.1$ the oscillations are stronger for $\beta_1 = 0.9$; for $\alpha = 0.01$ the profiles are smooth and the nonlocal curves overlap the discrete ones throughout.

Figure 13: Convergence trajectories of $\theta(t)$ for the nonlocal and discrete Adam models. These two plots show the evolution of the trajectory of $\theta(t)$ for the nonconvex function $\frac{1}{4}(\theta^2 - 1)^2$ with two initial conditions $\theta_0 = \pm 0.1$ for Adam.

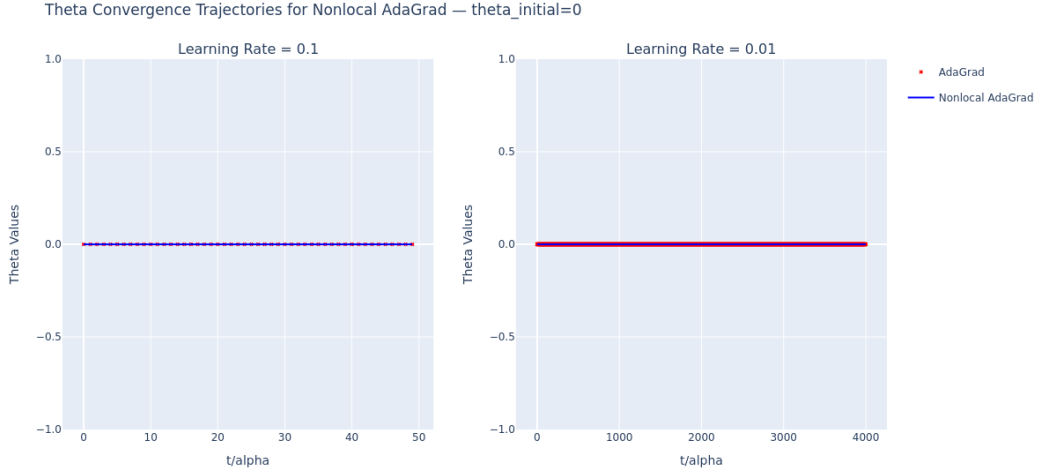


(a) **Second-moment trajectories of $v(t)$ for the nonlocal and discrete Adam models with positive initial-ization.** Second-moment trajectories $v(t)$ with $\theta_0 = 0.1$. Peak height and decay depend on the parameters: with $\alpha = 0.1$, $\beta_1 = 0.9$, $\beta_2 = 0.99$ yields the largest transient peaks, whereas $\beta_2 = 0.999$ produces smaller, flatter curves. For $\alpha = 0.01$, all settings display the characteristic bell-shaped peak followed by slow decay, and nonlocal and discrete curves nearly coincide.

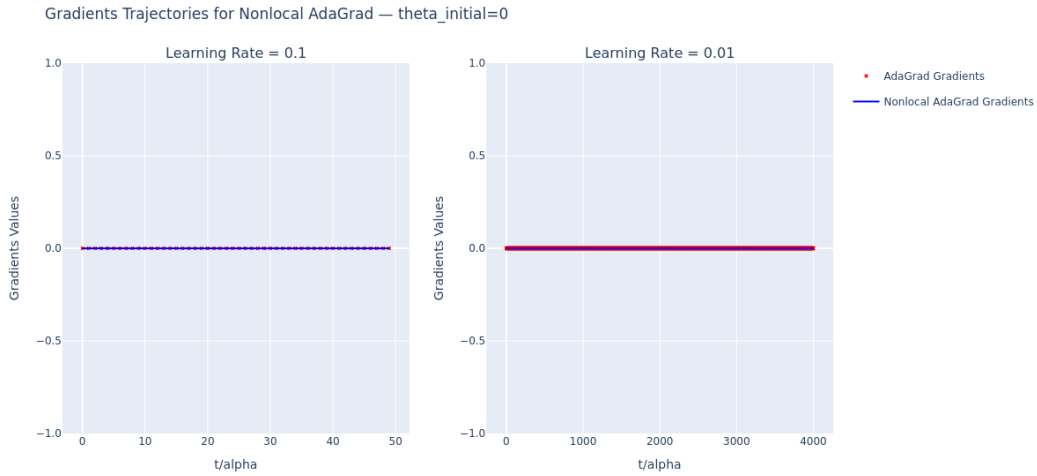


(b) **Second-moment trajectories of $v(t)$ for the nonlocal and discrete Adam models with negative initial-ization.** Second-moment trajectories $v(t)$ with $\theta_0 = -0.1$. Same qualitative pattern as in Fig. 14a: larger peaks for $\beta_2 = 0.99$ and much lower values for $\beta_2 = 0.999$. Agreement between nonlocal and discrete models is very close, especially for the smaller learning rate.

Figure 14: **Convergence trajectories of $\theta(t)$ for the nonlocal and discrete Adam models.** These two plots show the evolution of the trajectory of $\theta(t)$ for the nonconvex function $\frac{1}{4}(\theta^2 - 1)^2$ with two initial conditions $\theta_0 = \pm 0.1$ for Adam.



(a) **Parameter trajectories of $\theta(t)$ for the nonlocal and discrete AdaGrad models with zero initialization.** Theta trajectories (AdaGrad vs. Non-local AdaGrad) for the nonconvex function $\frac{1}{4}(\theta^2 - 1)^2$ for the initial value $\theta_0 = 0$.



(b) **Gradient trajectories of $\theta(t)$ for the nonlocal and discrete AdaGrad models with zero initialization.** Gradient trajectories (AdaGrad vs. Non-local AdaGrad) for the nonconvex function $\frac{1}{4}(\theta^2 - 1)^2$ for the initial value $\theta_0 = 0$.

Figure 15: Equilibrium trajectories of $\theta(t)$ and $G(t)$ for the nonlocal and discrete AdaGrad models. These two plots show the evolution of the trajectory of $\theta(t)$ with the gradient $G(t)$ for the nonconvex function $\frac{1}{4}(\theta^2 - 1)^2$ under AdaGrad. As can be observed, since the system starts directly at the unstable local maximum $\theta_0 = 0$, it remains unchanged. However, even an arbitrarily small perturbation would cause it to converge to one of the local minima. We also present the discrete case, and, as can be seen, the behavior of the continuous system is completely identical.

REFERENCES

- Ferran Alet, Dylan Doblar, Allan Zhou, Josh Tenenbaum, Kenji Kawaguchi, and Chelsea Finn. Noether networks: meta-learning useful conserved quantities. *Advances in Neural Information Processing Systems*, 34:16384–16397, 2021.
- Hédy Attouch, Jérôme Bolte, Patrick Redont, and Antoine Soubeyran. Proximal alternating minimization and projection methods for nonconvex problems: An approach based on the kurdyka-łojasiewicz inequality. *Math. Oper. Res.*, 35(2):438–457, May 2010. ISSN 0364-765X. doi: 10.1287/moor.1100.0449. URL <https://doi.org/10.1287/moor.1100.0449>.
- I. Barbalat. Systemes d’équations différentielles d’oscillations non lineaires. *Revue Mathématique Pures et Appliquées*, 4:267–270, 1959.
- Heinz H. Bauschke and Patrick L. Combettes. *Convex Analysis and Monotone Operator Theory in Hilbert Spaces*. CMS Books in Mathematics. Springer, Cham, 2 edition, 2017. ISBN 978-3-319-48310-4. doi: 10.1007/978-3-319-48311-1.
- Léon Bottou. Large-scale machine learning with stochastic gradient descent. In Yves Lechevallier and Gilbert Saporta (eds.), *Proceedings of COMPSTAT’2010*, pp. 177–186, Heidelberg, 2010. Physica-Verlag HD. ISBN 978-3-7908-2604-3.
- Stephen P Boyd and Lieven Vandenberghe. *Convex optimization*. Cambridge university press, 2004.
- Ricky TQ Chen, Yulia Rubanova, Jesse Bettencourt, and David K Duvenaud. Neural ordinary differential equations. *Advances in neural information processing systems*, 31, 2018.
- Miles Cranmer, Sam Greydanus, Stephan Hoyer, Peter Battaglia, David Spergel, and Shirley Ho. Lagrangian neural networks. *arXiv preprint arXiv:2003.04630*, 2020.
- John Duchi, Elad Hazan, and Yoram Singer. Adaptive subgradient methods for online learning and stochastic optimization. *Journal of Machine Learning Research*, 12(61):2121–2159, 2011.
- Weinan E. A proposal on machine learning via dynamical systems. *Communications in Mathematics and Statistics*, 5(1):1–11, 2017. doi: 10.1007/s40304-017-0103-z.
- Bálint Farkas and Sven-Ake Wegner. Variations on barbălat’s lemma. *The American Mathematical Monthly*, 123(8):825, 2016. ISSN 0002-9890. doi: 10.4169/amer.math.monthly.123.8.825. URL <http://dx.doi.org/10.4169/amer.math.monthly.123.8.825>.
- F.R. Gantmakher. *Lectures in Analytical Mechanics: Translated from the Russian by George Yankovsky*. Mir Publishers, 1970.
- Claudio A. Gelmi and Héctor Jorquera. Idsolver: A general purpose solver for nth-order integro-differential equations. *Computer Physics Communications*, 185(1):392–397, 2014. ISSN 0010-4655. doi: doi.org/10.1016/j.cpc.2013.09.008.
- Samuel Greydanus, Misko Dzamba, and Jason Yosinski. Hamiltonian neural networks. *Advances in neural information processing systems*, 32, 2019.
- Carlos Heredia. Nonlocal lagrangian formalism, 2023.
- Carlos Heredia and Josep Llosa. Non-local lagrangian mechanics: Noether’s theorem and hamiltonian formalism. *Journal of Physics A: Mathematical and Theoretical*, 54(42):425202, September 2021. ISSN 1751-8121. doi: 10.1088/1751-8121/ac265c.
- Geoffrey Hinton. Lecture 6: Training a multilayer neural network. University of Toronto, 2012. CSC321: Neural Networks for Machine Learning.
- Hamed Karimi, Julie Nutini, and Mark Schmidt. Linear convergence of gradient and proximal-gradient methods under the polyak-łojasiewicz condition. In Paolo Frasconi, Niels Landwehr, Giuseppe Manco, and Jilles Vreeken (eds.), *Machine Learning and Knowledge Discovery in Databases*, pp. 795–811, Cham, 2016. Springer International Publishing. ISBN 978-3-319-46128-1.

-
- H. K. Khalil. *Nonlinear Systems*. Prentice Hall, Upper Saddle River, NJ, 3rd edition, 2002.
- Diederik P Kingma and Jimmy Ba. Adam: A method for stochastic optimization. *arXiv preprint arXiv:1412.6980*, 2014.
- Nikola B Kovachki and Andrew M Stuart. Continuous time analysis of momentum methods. *Journal of Machine Learning Research*, 22(17):1–40, 2021.
- Qianxiao Li, Cheng Tai, and Weinan E. Stochastic modified equations and adaptive stochastic gradient algorithms. In Doina Precup and Yee Whye Teh (eds.), *Proceedings of the 34th International Conference on Machine Learning*, volume 70 of *Proceedings of Machine Learning Research*, pp. 2101–2110. PMLR, 06–11 Aug 2017.
- Ilya Loshchilov and Frank Hutter. Decoupled weight decay regularization. *arXiv preprint arXiv:1711.05101*, 2017.
- Yurii Nesterov. *Introductory Lectures on Convex Optimization: A Basic Course*, volume 87 of *Applied Optimization*. Springer, 2004. ISBN 978-1-4020-7553-7. doi: 10.1007/978-1-4419-8853-9.
- B.G. Pachpatte. Chapter one - linear integral inequalities. In B.G. Pachpatte (ed.), *Inequalities for Differential and Integral Equations*, volume 197 of *Mathematics in Science and Engineering*, pp. 9–97. Elsevier, 1998. doi: [https://doi.org/10.1016/S0076-5392\(98\)80003-9](https://doi.org/10.1016/S0076-5392(98)80003-9).
- Orlando Romero, Mouhacine Benosman, and George J. Pappas. Ode discretization schemes as optimization algorithms. In *2022 IEEE 61st Conference on Decision and Control (CDC)*, pp. 6318–6325, 2022. doi: 10.1109/CDC51059.2022.9992691.
- Sebastian Ruder. An overview of gradient descent optimization algorithms. *arXiv preprint arXiv:1609.04747*, 2016.
- David E. Rumelhart, Geoffrey E. Hinton, and Ronald J. Williams. Learning internal representations by error propagation. 1986.
- Lars Ruthotto and Eldad Haber. Deep neural networks motivated by partial differential equations. *Journal of Mathematical Imaging and Vision*, 62(3):352–364, 2020. doi: 10.1007/s10851-019-00903-1.
- Justin Sirignano and Konstantinos Spiliopoulos. Stochastic gradient descent in continuous time. *SIAM Journal on Financial Mathematics*, 8(1):933–961, 2017.
- Weijie Su, Stephen Boyd, and Emmanuel J. Candès. A differential equation for modeling nesterov’s accelerated gradient method: Theory and insights. *Journal of Machine Learning Research*, 17(153):1–43, 2016.
- Hidenori Tanaka and Daniel Kunin. Noether’s learning dynamics: Role of symmetry breaking in neural networks. *Advances in Neural Information Processing Systems*, 34:25646–25660, 2021.
- Andre Wibisono, Ashia C Wilson, and Michael I Jordan. A variational perspective on accelerated methods in optimization. *proceedings of the National Academy of Sciences*, 113(47):E7351–E7358, 2016.
- Emanuele Zappala, Antonio Henrique de Oliveira Fonseca, Andrew Henry Moberly, Michael James Higley, Chadi Abdallah, Jessica Cardin, and David van Dijk. Neural integro-differential equations, 2022.
- Ștefan Cobzaș, Radu Miculescu, and Adriana Nicolae. *Lipschitz Functions*, volume 2241 of *Lecture Notes in Mathematics*. Springer, Cham, Switzerland, 2019. ISBN 978-3-030-16488-1. doi: 10.1007/978-3-030-16489-8.